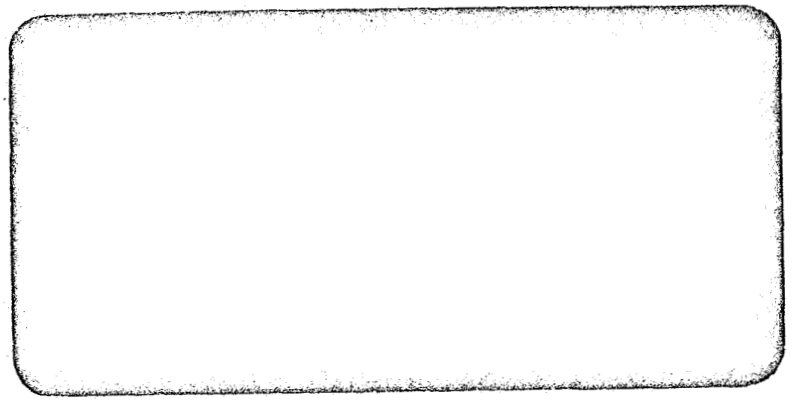

WYLE LABORATORIES
TESTING DIVISION, HUNTSVILLE FACILITY

FACILITY FORM 602

N68-13394 (ACCESSION NUMBER)	(THRU)
70 (PAGES)	0 (CODE)
CR 91237 (NASA CR OR TMX OR AD NUMBER)	03 (CATEGORY)

WYLE LABORATORIES - RESEARCH STAFF

REPORT WR 67-3

SHADOWGRAPH VISUALIZATION OF NOISE FROM COLD SUPERSONIC JETS

by

M. V. Lowson

Submitted Under Contract NAS 8 - 11312

Prepared by M.V. Lowson
M.V. Lowson

Approved by R.C. Potter
R.C. Potter
Project Manager

Approved by L.C. Sutherland
L.C. Sutherland
Assistant Director Research

Date January 31, 1967

COPY NO. 26

CASE FILE LOAN DOCUMENT
CASE FILE LOAN DOCUMENT

F68-476 Putnam

DOCUMENT REQUEST

NASA Scientific and Technical Information Facility
operated for the National Aeronautics and Space Administration by Documentation Incorporated
Post Office Box 33 College Park, Maryland 20740

DOCUMENT REQUESTED

A. NASA ACCESSION NUMBER:	B. NACA/NASA REPORT NUMBER:
1 N68-13394	OR CR 91337

C. (PLEASE DO NOT WRITE IN THIS SPACE)

D. COPY TYPE REQUESTED: ☐ MICROFICHE ☒ FULL SIZE (16)

REQUESTER IDENTIFICATION

E. REQUESTER'S FACILITY IDENT. NO.:	F. REQUESTER'S CONTRACT NO.:
17 4	

G. AUTHORIZED SIGNATURE AND DATE: Jean L Jones 5 Apr 68

FF No. 492 REV. DEC. 65

2. REPLY COPY

OTHER BIBLIOGRAPHIC INFORMATION

H. DOCUMENT TITLE: NOTICE: THE SHADOGRAPHS ARE NOT LEGIBLE IN THIS COPY. WE NEED CLEAR VIEWS OF THE SHADOWGRAPHS.

I. DATE OF REPORT:	J. AUTHOR(S):

K. CORPORATE SOURCE:	L. CORPORATE REPORT NO.:

M. **MAILING LABEL** (must be imprinted on all copies)

NASA-FRC
LIBRARY
P. O. BOX 273
EDWARDS, CALIF 93523

This document must be returned to the address shown below on or before 4-25-68.

Attn: Classified Supply Branch - Case File Clerk
NASA Scientific and Technical Information Facility
Post Office Box 33
College Park, Maryland 20740

Date: 4-19-68

MUST BE RETURNED
MUST BE RETURNED

SUMMARY

Shadowgraphs of the sound field from over and under expanded cold supersonic jets, both deflected and undeflected, are presented and analyzed. Appendices present the results from a simple theoretical model, and recommendations for additional tests. It appears that the radiation field from the supersonic part of the jet is of relatively high frequency and that the sound from the subsonic part of the jet is the principal contributor to the overall sound power. In the supersonic region the apparent order of significance of the noise sources is i) radiation from the nozzle, ii) radiation from shock-turbulence interaction within the jet flow, iii) Mach wave radiation. The significance of the first source is thought to be due to the small scale of the present experiments, and demonstrates the necessity for care in extrapolation of small scale acoustic results. The second source will not be present in perfectly expanded jet flows. The principal noise source from the deflected jet appears to arise from the jet-deflector intersection and associated shock pattern. It is suggested that Mach reflection of spherical pulses may be an important factor in determining the observed noise field. The possibility of near field noise within the jet being converted to far field noise outside the jet is also pointed out.

TABLE OF CONTENTS

LIST OF FIGURES

LIST OF FIGURES (Continued)

1.0 INTRODUCTION

At the present time little is known of the noise producting mechanisms in rocket exhaust flows. Even the best prediction methods rely strongly on empirical techniques (Reference 1). Early experimental work, (References 2 to 4) indicated that the major sources of noise came from the downstream subsonic portion of the rocket exhaust, and this observation was supported by the first theoretical analyses (Reference 5).

Theoretical study of the rocket exhaust flow has produced a number of interesting conclusions, which tend to suggest that the main noise producing part of the rocket exhaust is in the supersonic part of the flow. This theoretical work has not yet developed to the stage where it can be used for the prediction of rocket noise, mainly because of the complex and random nature of the flow field in the exhaust. The leading result of the theoretical studies of the noise is the suggestion that intense sound leaves the exhaust flow as "Mach waves" which may be crudely regarded as the ballistic shock waves shed by the turbulent eddies as they move supersonically downstream. The Mach wave concept was introduced by Phillips (Reference 6) and extended and considerably refined in a series of papers by Ffowcs Williams (References 7 to 10). Shadowgraph pictures of supersonic turbulence have confirmed the existence of Mach waves, although their relative importance in the noise field of the rocket exhaust has not been conclusively demonstrated. The Mach wave radiation field has a second important property (Reference 11). Because the acoustic field is highly directional there is little interference between the acoustic signals radiated from different parts of the flow. Thus, acoustic measurements close to the flow will reveal details of the turbulent mechanisms within the flow, giving a remote method for estimating the turbulence parameters within the supersonic flow.

Ffowcs Williams claims that the quadrupole noise emission, familiar in subsonic turbulent shear flows from the work of Lighthill (References 12 and 13) carries over into supersonic flows. Lighthill and Ffowcs Williams showed how the mean square sound pressure level radiated by a quadrupole source could be expressed as

$$\overline{p^2} \sim \frac{a_o^4 \ell^2}{r^2} \frac{M^8}{(1 - M \cos \theta)^5}$$

where ℓ is a typical flow dimension, r the distance of observer from the source, θ the angle between the direction of motion and the observer, and M the flow Mach number. When M is large, the fifth power of M in the denominator predominates, and thus, approximately,

$$\overline{p^2} \sim \frac{a_o^4 \ell^2}{r^2} \frac{U^3}{\cos \theta^5}$$

at large M, and θ not near 90°.

Thus, the familiar U^8 power law goes over into a U^3 law. This result is also observed in experiment. However, this agreement does not prove that the quadrupole radiation is the prime source of noise. Monopole, dipole, or even octupole and higher orders of noise sources all tend assymptotically to U^3 laws at high convection Mach numbers. The significance of lower order sources on low velocity jet noise has been pointed out by Ffowcs Williams and Gordon (Reference 14). It seems possible that these sources may also be significant in high velocity jets, particularly those of small scale.

Monopole noise is radiated by a jet simply due to the varying mass flow passing through the nozzle exit. The mass flow variation is, in turn, generally due to the turbulent boundary layer, but will be enhanced if significant free stream turbulence is present. Dipole noise radiation arises at the lip of the jet exhaust due to the boundary layer pressure fluctuations existing there. Quadrupole noise is the lowest order of sound radiated by the turbulent mixing process, but higher order octupole, etc., sources are also radiated, which can be legitimately neglected in subsonic analyses (Reference 5). All these sources of noise may be significant at supersonic speeds and will require careful study.

The equations above show an apparent singularity at $M \cos \theta = 1$. This is due to approximations introduced into the analysis, in particular, the neglect of finite eddy lifetime. However, a major increase in noise radiation can be expected at observation points which approach this Mach wave direction. A theoretical analysis using model correlations giving typical directivity patterns was presented by Ffowcs Williams (Reference 7). Unfortunately, the exact significance of the Mach wave radiation is not known. There is some question as to the frequency content of the Mach wave signal, and the amplitude of this radiation relative to that from the subsonic parts of the jet.

A further important question arises in the formation and decay of Mach waves. Intuitively it would be expected that Mach waves would arise from a summation of a number of individual spherical pressure pulses shed by the supersonic eddy. This model is normally used to describe how a shock wave arises in front of an aerofoil. However, Ffowcs Williams has suggested in a recent paper (Reference 9) that an opposite mechanism exists, with the sound being generated as Mach waves and developing far away from the source region into spherical waves. Probably both mechanisms are at work, and when these are combined with the familiar non-linear acoustic mechanisms of sound wave steepening and absorption, it becomes apparent that interpretation of the shadowgraphs, or of any results

relating to Mach waves, will be very difficult. The experiments discussed in later sections of the report are intended to supply more details of this Mach wave mechanism to assist analytical and empirical evaluation of the acoustic field.

In fact, there are two forms of acoustic radiation even from the supersonic part of the flow. The first is the "Mach wave" radiation discussed above, and the second is due to shock interaction in the flow. Practical supersonic exhausts do not operate in a perfectly expanded condition so that a shock structure exists within the flow. These shocks extend into the supersonic parts of the turbulent mixing layers, and therefore undergo unsteady interactions.

Turbulence in a supersonic flow may be regarded as consisting of three "modes", first demonstrated by Kovasznay (Reference 15). Fluctuations may occur in the vorticity, entropy, or sound modes, which can be identified alternatively as velocity, temperature, and pressure modes. The shock front couples these fluctuations together so that input of any one mode will generate fluctuations in all three in the downstream side. Thus, passage of any of these modes through the shock can generate sound, and the passage of a pattern of compressible turbulence through a shock can certainly be expected to generate substantial noise levels, as well as fluctuations in other modes passing downstream. The sound generated by the interaction has a significant near field (Reference 16) which will be considered later, and it appears that several interesting conclusions can be drawn from study of a very simple model of sound propagation inside and outside the supersonic flow. These theoretical considerations are presented in Appendix A.

Some previous related experimental work has been performed by other investigators (References 17 to 23). However, most of this work has been investigations of the discrete frequency noise generation by overpressure two-dimensional supersonic jets. This discrete frequency noise generation has been associated with an instability mechanism in the jet cell structure, first suggested by Powell (Reference 24). Although this problem is not the same as in the present case, sound waves were observed in the shadowgraphs of those investigations. It has been found that although an instability can occur in highly overpressure jets, this is rarely encountered in practice, except at very high altitudes.

2.0 EXPERIMENTAL APPARATUS

The experiments were performed at a base flow facility located out of doors at Marshall Space Flight Center. The facility was modified to allow the jet flow to be directed horizontally, and an available Model SI B vehicle was used as a final settling tank during the experiments. A general view of the experimental setup is shown in Figure 1. Seven of the nozzles on the model were closed off, and the flow of one nozzle only was considered. Preliminary experiments utilized a conical nozzle, the flow from which necessarily contained shocks. However, the major portion of the tests were run with a 1 inch exit diameter nozzle designed using the method of characteristics for a uniform shock free flow at Mach 2.5.

The flow from the nozzle was found to be perfectly expanded at Mach 2.47, and at this Mach number some weak shocks were still present in the flow. The program used to calculate the nozzle contours did not include any allowance for the nozzle boundary layer, however the small discrepancy between design and actual operating Mach number is more likely due to manufacturing errors. The static pressure at the nozzle exit was detected using a wall pressure tap at the lip of the nozzle, and the flow was taken to be perfectly expanded when the static pressure measured at this location was equal to the atmospheric pressure.

Shadowgraph pictures were made using a small diameter short duration (0.5 μs) spark source available at Marshall Space Flight Center. The spark source and film were positioned as shown in Figure 2. Kodak Royal Pan film was used throughout the tests. Cut film, 24 inches by 20 inches, was placed in a special holder. This holder included a suction system to keep the film in contact with the backing plate, and a remotely controlled shutter. During the taking of shadowgraph pictures, the spark source was triggered automatically when the shutter was fully open. To minimize fogging of the film during the opening of the shutter, all tests were run at night and, in addition, a light proof shelter was built around the jet flow. A venetian blind system positioned about 500 diameters away from the jet exit allowed the jet air to escape from the shelter.

Shadowgraphs of both deflected and undeflected jets were made. A photograph of the test setup for the undeflected jets is shown in Figure 1, and relevant dimensions are given in Figure 2. A photograph of the test setup for the deflected conditions is shown in Figure 3, and the relevant dimensions shown in Figure 4. A listing of the experimental conditions tested is shown in Tables 1 and 2. Only runs which resulted in successful shadowgraph pictures are shown. Undeflected jets were tested at varying pressure ratios (approximately at 200, 150, 100, 75, and 50 percent of the fully expanded pressure ratio). The acoustic field of the fully expanded jet was examined over a large area and also by means of oblique shadowgraphs (see Figure 2). Deflected jets were

examined at approximately 150, 100, and 75 percent of the fully expanded pressure ratio, and at various jet to deflector plate distances. At the maximum jet to deflector distance, deflector plate angle was varied from 30 to 60 degrees. For the deflected jet experiments, the film was mounted behind a 1/16 inch plexiglass sheet to prevent it from being blown from the holder.

All runs were made using air at atmospheric stagnation temperature, supplied from a pressurized tank. Facilities for raising the stagnation temperature to a maximum of 600 °F were available, but were not utilized during this phase of the experiments. No acoustic measurements were made.

3.0 RESULTS

In this section, the features of the flow and acoustic fields observed in the shadowgraph pictures are described, and some of the more obvious conclusions are drawn. A more detailed analysis of the results is given in the next section. Each of the photographs taken for the undeflected case shows features of interest. Since the object of the experiments was to take shadowgraph pictures visualizing the flow, all these undeflected pictures are shown in Figures 5 to 14. The visualizations for the deflected cases were often similar to each other, and only a selection is presented here in Figures 15 to 21. An example of the field obtained with the conical nozzle used for the preliminary tests is shown in Figure 22, and results from some tests performed at Langely Research Center on the hot jets are shown in Figures 23 and 24.

Previous work at Wyle Laboratories, reported in Reference 25, had demonstrated the significance of film to flow distance on resolution. This effect was again observed in the tests on the conical nozzle during the preliminary phases of the present tests. Little of the acoustic field could be observed on shadowgraphs taken with the film a few inches from the jet, while shadowgraphs taken several feet from the jet showed a confused pattern. The setup shown in Figure 2 was adopted for all the pictures shown here, with a film to flow distance of 18 inches being chosen for optimum resolution.

All the photographs exhibited some overall fog, but extensive modifications to the test setup would have been required to remove this, and it has not compromised the analysis of the pictures.

Figure 25 shows a comparative view of the flows observed at the five pressure ratios studied in the undeflected experiments. The observation of a shock cell structure is consistent with all previous work, and a detailed discussion of these effects was presented in Reference 26. In the present experiments, the principal interest is in the acoustic field radiated by the various jet flows.

Figures 5 through 9 show the total field of the undeflected jet at several pressure ratios, with pressure ratio increasing in successive pictures. Figure 7 gives the field resulting from the ideally expanded jet at an exit pressure ratio of unity. Figure 26 gives a diagramatic representation of the field of Figure 7 to assist interpretation of the features observed. That the jet is near ideal expansion is confirmed by the apparent straightness of the jet edges (compare in Figure 25). Figure 7 shows a fairly clear boundary between the inner and outer regions. This is assumed to correspond to a view through the laminar core of the jet, upon which is superimposed the surrounding turbulence. No value of core length can be inferred from the photographs, but the predicted length of the laminar core using data from Reference 26 would be about 16 diameters. The

predicted length of supersonic core would be of the order of 40 diameters.

Close to the nozzle, Figure 7 shows a closely spaced series of circular arcs, clearly centered on the nozzle lip. As we progress to the edge of the picture at the corner away from the nozzle, more intense waves appear, and the spacing between these shock waves is much larger than that between the waves close to the lip. It is noteworthy that many of the shock waves in the photograph split into two distinct less intense waves at their termination, as shown in Figure 26. The angular region (centered on the nozzle) in which the intense waves appear is limited in extent and virtually all the intense waves observable in Figure 7 appear to have arisen from the first two or three diameters of the jet flow. In the downstream direction from the intense waves, a second phenomenon can be observed. This is the appearance of "packets" of waves. These wave packets appear to be inclined at a smaller angle to the jet than the more intense phenomena.

Figure 5 shows an underpressure jet. The same general pattern near to the lip of the nozzle,as in the ideally expanded jet of Figure 7, can be seen. However, it appears that the field is less intense since the shock waves appear to be weaker and to appear further away from the nozzle. A second feature, clearly apparent in the original 20 x 24 in. plates, is a secondary spherical radiation centered close to the intersections of the core shocks with the turbulent shear layer. This feature is observed in all shadowgraphs taken of flows containing core shocks, and is most clearly apparent in the reproductions of this report in Figure 22. This form of radiation was also observed by Ollerhead in Reference 25. A number of the shock waves visible in Figure 5 may also be attributed to this radiation, although it is often difficult to be certain as to the exact center of these shocks. It is of interest to note that virtually all the intense waves visible far from the nozzle are spherical in form. Figure 6 shows a jet operating at a pressure ratio midway between that of Figures 5 and 7 and the sound field pattern can be seen to resemble a mixture of the two cases.

Figure 8 shows an overpressure jet. Again the radiation centered on the nozzle lips is evident, and the spherical radiation centered on the intersection of the core shocks with the turbulent shear layer is also present. The sound field appears to be more intense in this case, as evidenced by the stronger shocks appearing closer to the nozzle. Figure 9 shows a jet operating at about 100 percent overpressure. The same two radiation features are evident, although intensity of the sound field in the shadowgraph is reduced. In general, the intensity of the sound fields observed in the shadowgraph pictures supports the intuitive idea, and the acoustical data, that sound intensities increase with increase in pressure ratio. However, no clear conclusions can be drawn since neither exposure, development, or printing of the film was under photogrammetric control.

Figures 7, 10, 11, and 12 together constitute an extended survey of a large area of the acoustic field of the ideally expanded jet. The conditions for each figure may be found by reference to Table 1 and Figure 2. Each shadowgraph was taken on a different run, so that exact continuity between the figures is not to be expected. Figure 10 shows the region of the jet immediately downstream of that shown in Figure 7. Little evidence of acoustic radiation from this portion of the jet is visible, even though the jet would be expected to still be supersonic here from the data of Reference 26. However, radiation from the upstream portion of the jet is crossing the top part of the shadowgraph. Again, the two forms of radiation observed for the fully expanded jet (the shock waves and the wave "packets") are visible.

Figure 11 shows the field immediately above Figure 10. Shock waves are visible passing all the way across the field. It is very noticeable that the average distances between these shock waves has spaced out compared to those apparent in Figure 7. Figure 12 gives the field immediately above that of Figure 7. Even on the original 20 x 24 in. plate little acoustic radiation was visible, save for some weak effects in the downstream corner nearest the jet.

Figures 13 and 14 show shadowgraphs taken from an oblique direction. Details of this setup are given in Figure 2. Figure 13 gives the 30 degrees oblique case and the obvious feature of this picture is the spherical shock waves centered approximately on the jet exit. Figure 14 shows the result of the 45 degrees oblique shadowgraph. Little is visible compared to Figure 13, and these two pictures give rise to some interesting conclusions which are discussed in the next section.

Figures 15 to 21 show shadowgraphs of various deflected cases. Unfortunately, the film for these cases did not quite pick up the outline of the jet exit. However, this is not thought to be very significant, as the flow and acoustic fields near to the jet are undoubtedly the same as in the undeflected cases. The conditions for Figures 15 to 22 are shown in Table 2. The flow field observed in each case is quite similar, and only a selection of all the pictures taken is presented. The obvious feature of all these shadowgraphs is the intense spherical radiation eminating from the point of jet deflection. A second feature is the rather blurred appearance of the shadowgraph at this point. This is thought to be due to the deflected flow striking the plexiglass sheet in front of the film at this point. Unfortunately this has resulted in the loss of any possible definition of shock structure on the deflector plate. An interesting feature of all the figures is the radiation centered on the upper edge of the deflector plate, presumably due to diffraction of the noise field around the plate edge. In each case, the portion of the jet upstream of the deflector seems to be radiating the same field as in the undeflected case. Upon this is superimposed the intense radiation from the jet-deflector intersection point.

In all the shadowgraphs, some additional shocks appear in the acoustic field; this is particularly clear in Figure 17. Presumably these are associated with shocks within the flow which are not visible on the shadowgraph. A particularly interesting set of shocks appears in Figure 19. At the downstream end of the jet,shocks are visible apparently propagating in the upstream direction. These have been tentatively associated with radiation from the bottom end of the deflector plate, not visible in the shadowgraphs. An equivalent set of waves can be discerned in the original plate of Figure 21. Comparison of Figures 19, 20 and 21 shows that the direction of radiation of the intense sound arising at the intersection is a function of deflector angle. It is difficult to give any precise numerical value to this effect, but appears that the angle of maximum radiation should be at about 45 degrees to the deflector plate.

Figure 22 shows a shadowgraph taken during the preliminary tests with a conical nozzle. The nozzle was far from ideal, and the result appears to be that intense radiation occurs at each of the internal shock waves. Strong radiation also occurred from such points in Wyle Laboratories preliminary results on another (different) non-ideal nozzle shape (Reference 25). It appears that deviation from ideal nozzle shape causes more intense radiation from the core shocks. Figures 23 and 24 show a shadowgraph taken on a hot jet at Langley Research Center. There are several obvious differences between this picture and those taken during the present experiments on a cold jet. These will be discussed in more detail in the next section.

4.0 ANALYSIS OF THE RESULTS

It is of interest to ask, first of all, exactly what part of the field is observed on a shadowgraph. The acoustic waves may be assumed to radiate outwards from the jet, so that a section through the wave field will reveal a series of circles centered on the jet as shown in Figure 27. If a simple point spark source is used, then the shadowgraph record is a result of the interaction of the conical shadowgraph field with the circular segments of the Mach waves. Mach waves will appear on the shadowgraph if part of the wave is tangential to a line passing through the spark source. If the waves are circular in section, this implies that the shadowgraph will record those waves which lie on a locus of points such that the angle subtented by the source and jet (SMJ in Figure 3) is 90 degrees. This locus is a circle with the source and jet as diameter, as shown in Figure 27. If Mach waves are not perfect circles centered on the jet axis, the above circle would define the region of maximum definition of the Mach wave field recorded on the shadowgraph. In fact, if the centers of the circles can all be assumed to lie within the jet, and the shadowgraph only records the waves to which it is tangential, then the only waves recorded will be in a region one jet diameter wide centered on the circle of maximum definition. This region is outlined by dotted lines in Figure 27. In the present experiments the source to jet distance was 96 inches, so that the above effects are not expected to be significant.

From the shadowgraphs, it seems that there are three sources of noise radiation from the jet:

i) spherical radiation centered on the nozzle exit,
ii) spherical radiation centered on shock-turbulence intersections, and
iii) acoustic "wave packets".

The original object of the experiments was to define the significance of the "Mach wave" field. Up to this point, it has not been possible to define this field with any precision. However, here a re-examination of Figure 7 is helpful. The acoustic "wave packets" occurring beneath the intense radiation centered on the nozzle have already been noted. It is tempting to associate each packet with the acoustic radiation from a single eddy. The direction of propagation of these packets is very clear, and towards the downstream side of Figure 7 a shock wave appears which seems to be a member of this family. (The approximate location of this wave is shown in Figure 26.) The typical angle of shock waves arising from the spherical radiation is about 47 degrees to the jet axis (see Table 3) and this angle increases towards the axis. The particular shock wave referred to above has an angle of about 42 degrees and, furthermore, it seems to be parallel to the acoustic wave packets. It is thought that this shock wave is a genuine "Mach wave" which has arisen from a coalescence of acoustic waves generated by a single eddy. At an earlier time, this

Mach wave is assumed to have resembled the wave packets observed nearer to the flow. The Mach wave is presumed to have formed several exit diameters from the flow because of the relatively low Mach number of the flow relative to the atmosphere (see Table 3).

The crucial evidence in this case is the difference in wave angle. Careful study of the original prints shows several other waves at approximately the same angle, particularly in the extended area coverage of Figures 10 and 11. Because the angle of these "Mach waves" is less than that of the waves centered on the nozzle, the two sets of waves must be expected to cross each other far out in the flow, and this can be seen in Figure 11. Several angular measurements of apparent Mach waves were made on the original plates and these suggested a slight steepening for the further downstream waves. This would be consistent with the idea that the eddies giving rise to the waves were moving more slowly further downstream.

The typical split found at the end of many of the shocks, observed in the spherical radiation, (see Figure 26) has also suggested several very interesting ideas. These are associated with the Mach reflection condition for incident shock waves. Figure 29 shows the general effect. When a shock wave strikes a surface, it is found, both theoretically and experimentally, to undergo either "regular" or "Mach" reflection (Reference 27). For small angles of incidence or high shock strength, regular reflection occurs. For sufficiently high angles of incidence (near grazing) or low strengths, it is found that a simple combination of two shocks cannot satisfy the boundary conditions and a third shock, the "Mach stem" is required. The strength of the third shock can be more than double that of the incident shock. A further "contact discontinuity" line also occurs, across which there is a jump in temperature. The theoretical limiting angle for various shock strengths is shown in Figure 29. When two equal spherical waves meet, as shown in Figure 29, then the initial effect will be a regular reflection, as shown. However, as the process develops, the angle of local incidence gradually increases and, sooner or later, dependent on the strength of the shock, a Mach reflection will occur and, for spherical shocks, a Mach disc will appear. (A similar process occurs in underpressure supersonic jets and a Mach disc is visible in the center of the jet flow in Figure 5.) Thus, at a sufficiently late stage in the process, the Mach disc will dominate the observed field with two closely spaced spherical waves arising from its edges. This final picture bears a remarkedly close resemblance to the split end configurations observed in the shadowgraph fields.

It is somewhat surprising to find that a weak, essentially acoustic, effect must be explained by recourse to a complete shock wave analysis. The theoretical prediction of this effect for weak shocks is clear from Figure 30, but it is helpful to consider the simple acoustic case to obtain further justification. Consider the reflection of an incident acoustic wave from a wall (as sketched in the

regular reflection case of Figure 29). It is well known that the strength of the reflected wave is equal to that of the incident. However, it is also clear that at grazing incidence, there will be no reflected wave. Thus, we predict that the strength of the reflected wave is identically equal to that of the incident waves at all angles of incidence up to 90 degrees, when it drops discontinuously to zero. This is unreasonable, and in fact, if the acoustic wave has any finite strength, this does not occur. A more exact theory predicts a smooth transition between the two conditions.

It appears that this Mach reflection condition will occur in practice and must be expected in the radiation from supersonic jets. The interaction of unequal strength waves will give rise to essentially the same, but distorted, pattern. Further evidence of its applicability in this case comes from a closer examination of typical split end shock waves. During the initial study of these waves it always seemed surprising that the two circles combining at one end of the shock wave did not reappear where expected at the other end of the split. Some definite displacement could be observed relative to the expected position. The arguments above make it clear that the two weak circular shocks joining at one end of the Mach stem are in fact the original wave and its reflection, and so reappearance of the original circular path would not be expected. It would be of distinct interest to perform an analysis of the Mach reflection of two weak spherical waves. It seems that the analysis could reveal much about the relation of shock length to strength, and on the effects of multi-interacting flows. Unfortunately, it was found that the Mach reflection of weak waves is one of the unsolved paradoxes of modern aerodynamic theory. (Reference 28.) It seems that while theory gives excellent experimental agreement for the strong shock case, there are significant differences for the interaction of weak waves at these large angles. No satisfactory explanation of this disagreement seems to have been advanced. Hopefully, the need for more definite results in this field will spur a further advance.

This discussion does not explain why the observed shock waves have a characteristic direction. Interaction of waves from different eddies in the flow could give rise to Mach reflections at virtually any angle. Thus, it must be assumed that each observed strong wave is the result of the summation of waves from a single eddy emitted at various times. The familiar arguments for supersonically convected sources will then give the directionality. Table 3 gives the typical measured directions of the intense spherical nozzle radiation, the equivalent convection Mach numbers, and the nozzle exit Mach numbers relative to the air. The latter figures were calculated assuming adiabatic expansion from ambient stagnation temperature and the known stagnation pressure, using the well known supersonic flow results (Reference 29). It does appear that the equivalent convection Mach number rises with jet exit Mach number, but it is difficult to draw any firm conclusion, because of the wide scatter in measured angles. Certainly the cut off angle of the nozzle radiation does not correspond

t is difficult to understand the exact mechanisms
fective angle to appear. Typically, the wave
/ of about 85 percent of the jet exit

the nozzle spherical radiation. The "Mach waves"
ded jet were at an angle of 42 degrees, corre-
90 percent of the jet exit velocity. The shadow-
n of W. Mayes at Langley Research Center, shown
24, also show what appear to be Mach waves.
e defined reasonably well and correspond to a
0 percent of the jet velocity. The wave angles
ge, but near the flow they correspond to a con-
ercent of the jet velocity. (See also Table 3.)
out the typical convection velocities of Mach
drawn. However, it should be noted that all these
red from theory. It appears that only the faster
ute to Mach wave radiation, in spite of the fact
by virtually any criterion reaches a peak at the
e convected velocity is equal to half the jet

the radiation field appears from the comparison
graphs available several years ago showed the
on the nozzle. However, the apparent wave-
was such that frequencies of over a megacycle
red that this field was not of practical significance.
rion field far from the nozzle has formed into
he order of the jet exit diameter apart. Several
g sound spectra for supersonic jets are available
shows the peak sound power to occur at
e frequency, D is the exit diameter,and a_e is
For the present cold jets,Figure 11 suggests an
$\sim$ 1.5. Thus, the observed radiation is an order
quency peak but is nevertheless at a frequency
nificance on a full scale engine. This also sug-
k arises from noise radiation from the downstream
greement with previous empirical analyses (for
contradiction to the theoretical arguments put

lique shadowgraphs has also yielded some inter-
ese experiments was to attempt to take shadow-
the Mach wave so that simultaneous

shadowgraphs of the same Mach wave field would reveal the relative lateral extent (Reference 30). Since the Mach wave angle could not be defined properly when these pictures were taken, it was decided to arbitrarily take the pictures at 30 degrees and 45 degrees, with the results shown in Figures 13 and 14. These results were initially very surprising since they were not consistent with the anticipated Mach wave field, which would consist of a series of cones of the same vertex angle. However, Figure 30 shows how the observed results are consistent with a field of spherical shocks of limited angular extent.

Figure 30a shows a side view of the spherical field. Although waves could exist all around the shaded area, they will only be visible in the shadowgraph where they lie tangential to a straight line passing through the light source. Thus, only the heavily marked edges of the field will appear in the shadowgraph. As the point of observation is moved around (corresponding to an oblique shadowgraph case) the extent of the observed edges increases as shown in Figure 30b until in Figure 30c a complete circular pattern will be observed. This case, Figure 30c, corresponds to the 30 degrees oblique case of Figure 13. Further moving around, as in Figure 30d, will diminish and remove any trace of the wave field in the shadowgraph, and little is visible in Figure 14. Thus, the field observed in Figure 13 shows, first of all, that the acoustic field is spherical in character. Secondly, Figure 30c shows how the observed field will still be centered on its actual center of curvature. The extensive spherical waves visible in Figure 13 are clearly centered at or near the jet exit. It therefore appears that a major part of the observed noise field for this jet, comes directly from the exit, and is presumably monopole or dipole noise arising from the turbulent boundary layer. This result is probably due to the small scale of the jet. Therefore this suggests caution applying directional measurements made with small jets to full scale cases.

5.0 CONCLUSIONS

The present experiments have revealed a considerable amount of qualitative and some quantitative information on the noise radiation by supersonic jets. It is concluded:

1) The most significant source of noise from the undeflected jets observed in the present experiments was a spherical radiation centered on the nozzle exit.

2) This radiation is thought to be associated with the turbulence at the jet exit, and is probably emphasized by the small scale of the present experiments.

3) Therefore caution should be exercised in extrapolating small scale acoustic results, particularly directionality, to the full scale case.

4) The second most significant source of noise was spherical radiation centered on the intersections of shocks in the jet flow with the jet turbulence. This source is thought to be of practical significance.

5) The shock-turbulence noise appears to be of additional significance in the flow from non-ideally contoured exit nozzles.

6) The least significant source of noise observed was the Mach wave radiation. This may be due to the use of cold jets in the present study.

7) The observed intensities increased with increase in pressure ratio.

8) The principal mechanism of formation of the observed shock waves is due to Mach reflection of individual spherical pressure pulses. This suggestion offers several ideas for theoretical development.

9) A secondary mechanism for the appearance of shock waves is probably nonlinear acoustics.

10) Cut-off angles for the nozzle radiation correspond to a convection velocity of about 85 percent of the jet velocity.

11) No definite convection velocity for the Mach wave generating eddies can be laid down, but it does appear to be higher than 70 percent of the jet velocity.

12) The observed frequency of the noise from the supersonic portion of the jet appears to be about an order of magnitude above the peak frequency found in acoustic measurements.

13) Therefore, radiation from the supersonic region is of distinct practical importance, but the predominant contribution to the low frequency noise is thought to be due to the subsonic parts of the exhaust flow.

14) The jet-deflector interaction is the dominant source of noise in deflected jets.

15) This radiation has a maximum very roughly at 45 degrees to the deflector plane.

In addition, theoretical work in Appendix A has shown many of the general effects of the flow parameters, including the possible significance of shock - turbulence interaction as a source of noise. The need for additional experiments is clear, and a complete set of tests is laid out in Appendix B. This includes acoustic studies, and more detailed tests designed to reveal additional features of the mechanisms at work in the acoustic field.

REFERENCES

1. Potter, R. C., and Crocker, M. J., "Acoustic Prediction Methods for Rocket Engines, Including the Effects of Clustered Engines and Deflected Exhaust Flow," NASA CR-566, 1966.

2. Mayes, W. H., Lanford, W. E., and Hubbard, H. H., "Near Field and Far Field Noise Surveys of Solid Fuel Rocket Engines for a Range of Nozzle Exit Pressures," NASA TN D-21, 1959.

3. Morgan, W. V., and Young, K. J., "Studies of Rocket Noise Simulation with Substitute Gas Jets, and the Effects of Vehicle Motion on Jet Noise," Wright Patterson, ASD-TDR-62-787, 1962.

4. Mayes, W. H., Edge, P. M., and O'Brien, J. S., "Near-Field and Far Field Noise Measurements for a Blow Down Wind Tunnel Supersonic Exhaust Jet Having about 475,000 Pounds of Thrust," NASA TN D-517, 1961.

5. Lighthill, M. J., "Jet Noise," A.I.A.A. Journal Volume 1, Number 7, pp 1507-1517, July 1963.

6. Phillips, O. M., "On the Generation of Sound by Supersonic Turbulent Shear Layers," Journal Fluid Mechanics, Volume 9, p. 1, 1960.

7. Ffowcs Williams, J. E., "The Noise from Turbulence Convected at High Speed," Phil. Trans. Roy. Soc. (London) A Number 1061, Volume 255, 1963.

8. Ffowcs Williams, J. E., and Maidanik, G., "The Mach Wave Field Radiated by Supersonic Turbulent Shear Flows," J. Fluid. Mech. Volume 21, Paragraph 4, pp 641-657, 1965.

9. Ffowcs Williams, J. E., "On the Development of Mach Waves Radiated by Small Disturbances," J. Fluid. Mech. Volume 22, Paragraph 11, pp 49-55, 1965.

10. Ffowcs Williams, J. E., and Maidanik, G., "Rocket Noise," Bolt Beranek and Newman Report 1324, October 1965.

11. Keast, D. N., and Maidanik, G., "Studies of the Near Field Noise Properties of a Small Air Jet," Bolt, Beranek and Newman Report 1272, February 1966.

12. Lighthill, M. J., "On Sound Generated Aerodynamically, Part 1, General Theory," Proc. Roy. Soc. A 211, 1952.

13. Lighthill, M. J., "On Sound Generated Aerodynamically, Part 2, Turbulence as a Source of Sound," Proc. Roy. Soc. A 222, 1954.

14. Ffowcs Williams, J. E., and Gordon, C. G., "Noise of Highly Turbulent Jets at Low Exhaust Speeds," AIAA Journal, Volume 3, Number 4, 1965.

15. Kovasznay, L. S. G., "Turbulence in Supersonic Flow," Jour. Aero. Sci., Volume 20, 1953.

16. Lowson, M. V., "The Fluctuating Pressures Due to Shock Interactions with Turbulence and Sound," Wyle Laboratories Research Staff Report Number WR 66-35, 1966.

17. Hammitt, A. G., "The Oscillation and Noise of an Overpressure Sonic Jet," J. AE. Sc. Volume 28, Number 9, pp 673-680, September 1961.

18. Davies, M. G., and Oldfield, D. E. S., "Tones from a Choked Axisymmetric Jet," Acustica, Volume 12, Part 1, pp 257-277, 1962.

19. Davies, M. G., "A Note on the Radiation and Cell Pattern of Choked Jets," J. Sound Vib., Volume 1, Number 3, pp 298-301, 1964.

20. Davies, M. G., "Acoustic Radiation of Discrete Frequency from a Choked Rectangular Jet," Ph.D Thesis University of Liverpool, England, October 1958.

21. Mayes, W. H., Unpublished Experiments at NASA Langley Research Center.

22. Sheeran, W. J., and Dosanjh, D. S., "Noise from Impinging Two Dimensional Underexpanded Jet Flows," JASA Volume 38, Number 3, pp 482-484, September 1965.

23. Sheeran, W. J., and Dosanjh, D. S., "Interacting Jet Flow Investigations," Syracruse University Research Institute, Report ME 1058-6309 I.

24. Powell, A., "On the Mechanism of Choked Jet Noise," Proc. Phys. Soc., Volume B 66, pp 1039-1056, 1953.

25. Ollerhead, J. B., "Some Shadowgraph Experiments with a Cold Supersonic Jet," Wyle Laboratories Research Staff, Report Number WR 66-44, 1966.

26. Ollerhead, J. B., "On the Prediction of the Near Field Noise of Supersonic Jets", Wyle Laboratories Research Staff, Report Number WR 66-45, 1966.

27. Courant, R., and Friedrichs, K. O., "Supersonic Flow and Shock Waves," Interscience Publishers, Inc., New York, 1948.

28. Birkoff, G., "Hydrodynamics, A Study in Logic, Fact, and Similitude," Dover Publications, Inc., New York, 1950.

29. Ames Research Staff, "Equations, Tables, and Charts for Compressible Flow," NACA Report 1135, 1953.

30. Lowson, M. V., "Shadowgraph Experiments in the Marshall Space Flight Center Jet Flow Facilities," Wyle Laboratories Research Staff, Technical Memorandum Number TM 66-15, 1966.

31. Ribner, H.S., "Convection of a Pattern of Vorticity Through a Shock Wave," NACA Report 1164, 1954.

32. Ribner, H.S., "Shock-Turbulence Interaction and the Generation of Noise," NACA Report 1233, 1955.

33. Potter, R.C., "Noise Field for Shadowgraph Model Rocket Experiments," Wyle Laboratories, TM 66-18, 1966.

TABLE 1

UNDEFLECTED JET CONDITIONS

Run Number	Stagnation Pressure psia	Atmospheric Pressure psia	Film Position (See Figure 2)	Figure Number
1/7	364.4	14.4	A	8
2/1	471.4	14.4	A	9
3/0	177.4	14.4	A	6
4/0	118.4	14.4	A	5
5/0	237.4	14.4	A	7
6/0	237.4	14.4	B	12
7/0	237.4	14.4	C	11
8/0	237.4	14.4	D	10
9/10	237.4	14.4	E (45 Degree Oblique)	14
11/0	239.6	14.6	F (30 Degree Oblique)	13

TABLE 2

DEFLECTED JET CONDITIONS

Run Number	Stagnation Pressure psia	Atmospheric Pressure psia	Distance Jet to Deflector (Inches)	Deflector Angle Degrees	Figure Number
12/1	233.5	14.25	4.25	45	15
13/0	364.5	14.15	4.25	45	
14/0	177.5	14.15	4.25	45	
15/1	232.5	14.15	8.0	45	16
16/0	364.5	14.15	8.0	45	17
17/0	177.5	14.15	8.0	45	18
18/1	232.5	14.15	16.0	45	19
19/0	364.5	14.15	16.0	45	
20/0	177.5	14.15	16.0	45	
21/1	232.5	14.15	16.0	60	20
22/0	232.5	14.15	16.0	30	21

TABLE 3

ANALYSIS OF RESULTS

Run Number	Stagnation Pressure psia	Pressure Ratio to 14.4 psi	Percent Expansion	M_J	M_0	θ_0 Degrees	θ_M Degrees	M_M	$\frac{M_M}{M_0}$	Figure Number
5/0	237.4	16.49	100	2.47	1.66	37.0	47	1.37	0.825	7
1/7	364.4	25.31	153	2.75	1.74	35.0	42	1.50	0.86	8
2/1	471.1	32.72	198	3.17	1.83	33.1	41	1.52	0.83	9
3/0	177.4	12.32	75	2.29	1.60	38.7	48	1.34	0.84	6
4/0	118.4	8.22	50	2.03	1.50	41.8	-	-	-	5
Langley 300°F	147	10.0	100	2.15	1.86	32.6	42	1.5	0.81	23
Langley 1200°F	147	10.0	100	2.15	2.75	21.3	30	2.0	0.73	24

M_J = Jet Velocity Divided by Speed of Sound in Jet

M_0 = Jet Velocity Divided by Speed of Sound in Free Field

θ_0 = Mach Angle Corresponding to M_0

θ_M = Typical Angle of Spherical Radiation Waves

M_M = Mach Number Corresponding to θ_M

APPENDIX A

GENERATION AND PROPAGATION OF SOUND FROM SUPERSONIC FLOWS

The approach followed in this section is based on a very simple model, which appears to give many features of interest on the noise generation by supersonic flows. The approach is particularly relevant to the noise generated by shock-turbulence interactions within the flow. It was suggested by a report by Kovasznay (Reference 15), who seems to have been one of the first to point out the significance of Mach waves for sound fields in supersonic flow.

Frequency Effects

Consider a plane sound wave in a supersonic flow as shown in Figure 31. The velocity of the wave normal to itself is

$$v_n = a + U \cos \alpha \qquad (1)$$

where a is the speed of sound in the flow, U the flow velocity, and α the angle between the velocity vector and the normal to the wave. Dividing equation (1) by the wavelength of the sound $2\pi/k$, where k is the wave-number, gives the frequency at a fixed observer as

$$f = (ak - Uk \cos \alpha)/2\pi$$

Now $k \cos \alpha = k_1$ the component of the wave number in the flow direction so that

$$K = k - Mk_1 \qquad (2)$$

where $K = 2\pi f/a$ and the Mach number $M = U/a$.

k is a scalar given by $k = k_1^2 + k_2^2 + k_3^2$ where suffices imply components in the three normal directions, with suffix 1 referring to the flow direction. It is of interest to construct equal observed frequency contours in wave number space. The expression given in (2) is symmetrical in k_2 and k_3, and for the present purposes k_3 will be put equal to zero. Contours of equal frequency (equal K) are therefore given by

$$k_2^2 = k_1^2 (M^2 - 1) - 2 k_1 MK + K^2 \qquad (3)$$

This equation represents a series of hyperbolae and typical contours for the case $M = 3$ are shown in Figure 32. $K = 0$ gives the degenerate case of a pair of straight lines, and all the curves tend asymptotically to a slope of $\cos \alpha = 1/M$, which corresponds to the Mach wave angle. It will be observed that only one of each pair of hyperbolae given by (3) is relevant to the present analysis.

Directionality

Now consider a supersonic jet having a square wave velocity profile. Sound generated within it passes into the free air after refraction at the interface. This is shown diagrammatically in Figure 32. At the interface the trace velocity of the internal and external sound fields will be identical if

$$\text{i.e., } v_T = U \quad \frac{a_1}{\cos \alpha} = \frac{a_0}{\cos \beta} \qquad (4)$$

where a_1 and a_0 are the speeds of sound inside and outside the jet, respectively. Figure 32 also shows lines of constant wave angle outside the jet calculated using Equation (6), assuming $M = 3$, $a_0 = a_1$. For example the line marked $\beta = 30$ degrees occurs at an angle in the jet of $\alpha = 122.7$ degrees, thus showing that waves traveling at an angle of 122.7 degrees in the jet will be refracted at the interface to travel at 30 degrees outside the jet.

Internal sound fields with trace velocities below the free field sound speed will not radiate, but generate only an exponentially decaying near field pressure pattern. For flow which is supersonic with respect to the external field all waves propagating forward within the flow will radiate. Backward facing waves will propagate provided

$$\cos \alpha > \frac{a_1}{a_0 + U} \quad \text{or} \quad \cos \alpha < \frac{a_1}{a_0 - U}$$

The first inequality corresponds to sound waves propagating backwards in and out of the flow, the second to sound waves directed backwards in the flow but being carried forwards by the flow velocity. It will be observed in Figure 32 that the $\beta = 0$ line occurs at $\alpha = 120$ degrees and $\beta = 180$ degrees at $\alpha = 104.5$ degrees. This corresponds to the fact that sound waves within the flow with values of α between these values are non-radiating. In particular it will be observed that Mach waves within the flow ($\alpha = 109.5$ degrees) do not radiate.

Since internal Mach waves are stationary with respect to the external flow this observation is not surprising.

It is now of interest to combine this analysis of the refracted wave angle with the previous analysis of observed frequency. The frequencies in the free field will be identical to those at a fixed observer in the jet. Thus the K contours in Figure 32 correspond to constant free field frequency contours. Combining the directionality lines with the frequency contours shows first of all that the Mach wave angle in the jet corresponds to a low frequency, so that low frequency sound within the flow does not propagate.

Furthermore, it is reasonable to suppose that there is a minimum wave number within the flow related to the flow dimension. Thus no contribution to the sound radiation process can be expected from the part of the wave number plane near the origin. It will therefore be observed that low frequency noise in the far field can be due only to low wave number components in the flow, and that this noise will propagate essentially at a small angle to the axis either forwards or backwards.

Figure 34 gives an alternative plot of the results and shows the wave number plane in free space (β-plane) with lines showing the original wave directions in the jet (α-plane) superimposed. It will be observed that a substantial part of the α-plane (the whole first quadrant) has been transformed into a segment of the β-plane between 75 and 90 degrees. From this observation it is natural to conclude that significant sound intensities would be observed in these free field directions. The frequency contours in the β-plane (Figure 32) also demonstrate that it is the high frequency sound which will be radiated in this direction.

Parallel to the effects observed in the β-plane it may also be observed that no radiation occurs in the free field Mach wave direction. In the case shown in Figure 34, with $M = 3$, sound radiation occurs for angles less than the free stream Mach wave angle. Reference to the β-plane frequency contours in Figure 32 shows that this is substantially a low frequency radiation. This radiation arises from the upstream facing sound waves in the flow being convected downstream at a speed faster than that of sound in the free field. This form of radiation can only occur when $U > a_0 + a_1$ (see Equation 4). Thus the present model for the sound generation process suggests a noticeable increase in low frequency sound at small angles to axis will occur for supersonic flows obeying the above inequality.

Near Field Effects

The analysis presented above considers only that part of the free field acoustic radiation arising as a result of acoustic radiation in the jet. In fact decaying

pressure fields within the jet can be converted into radiation pressure fields at the supersonic boundary. For a decaying "near field" pressure pattern phase speeds and wave directions can be defined, as for example in the work of Ribner (References 31 and 32). These phase speeds will be less than the speed of sound within the jet, but the "trace velocity" of these near field waves along the edge of the jet can be either greater or less than the speed of sound outside the jet. The analysis for any given phase velocity follows exactly the same lines as before, and the free field acoustic radiation will again be two peaks either side of the Mach wave angle, although in this case these peaks will be somewhat closer to the Mach wave angle.

Thus, the "gap" in radiation near the Mach wave angle observed in Figure 34 is filled in by radiation from the near field pressures generated within the jet. Recent work by Lowson (Reference 16) has shown how shock-turbulence interactions gives rise to near field pressures which may be locally as much as 20 dB higher than the far field radiation observed from the same interaction. Thus, it appears that this source of radiation can be significant in the total sound output from a supersonic jet. Numerical calculation of the effects here would be very difficult. However, one general feature of this radiation can be predicted. The pressure field arising from shock turbulence interactions will be most significant when it arises from interactions near the edge of the supersonic region. The pressure field from interactions well within the flow will have decayed significantly in the several wavelengths before it reaches the velocity jump, so that only a low frequency contribution would be expected.

Apparent Curvature

The equation relating the incident and refracting waves at the interface of a jet with a square velocity profile has already been derived (Equation 4) and discussed in detail. At this point it is of interest to go one stage further and consider the curvature of the sound waves as they propagate into the free stream. An analysis is presented below, and is an improved version of that reported by Ollerhead (Reference 25).

Figure 35 shows the passage of a wave at angle α in the jet, refracted an an angle β outside the jet. The angles α and β are related by Equation (4), derived above. Suppose the radius of the sound wave as it reaches the surface is

$$R_1 = d/\sin \alpha = a_1 t \qquad (5)$$

where d is the vertical distance of the source from the interface and t is time taken for the sound to reach the interface from its errosion point. Consider two sound waves angle $\delta\alpha$ apart, which reach the interface δt apart in time.

From Figure 35 it can be seen that

$$\delta x = \frac{R_1 \delta_\alpha}{\sin \alpha} + U\delta t = \frac{R_2 \delta_\beta}{\sin \beta} \tag{6}$$

also $\delta x \cos \alpha = a_1 \delta t + U \cos \alpha \ \delta t.$

Thus,

$$\left(a_1 + U \cos \alpha\right) \frac{R_1 \delta \alpha}{\sin \beta} = \frac{R_2 \delta \beta a_1}{\sin \beta}$$

or proceeding to the limit

$$R_2 = R_1 \left\{1 + \frac{U \cos \alpha}{a_1}\right\} \frac{\sin \beta}{\sin \alpha} \frac{d\alpha}{d\beta} \tag{7}$$

$d\alpha/d\beta$ can be evaluated from Equation (4) so that using the results in Equation (7), together with Equation (5) gives

$$\frac{R_2}{d} = \frac{\sin^2 \beta}{\sin^3 \alpha} \frac{\cos^2 \alpha}{\cos^2 \beta} \left\{\frac{1 + U \cos \alpha}{a_1}\right\} \frac{a_0}{a_1} \tag{8}$$

$$\frac{x}{d} = \left\{\frac{U}{a_1 \sin \alpha} + \tan \alpha - \frac{R_2}{d} \cos \beta\right\}, \quad y = - R_2 \sin \beta \tag{9}$$

where β is given in terms of α in Equation (4). Equation (9) gives the apparent source locations determined from examination of the shadowgraph field.

Conclusions

Sound generated within the flow, for instance by shock-turbulence interactions may well be significant. The propagation analysis given in this Appendix was based on a simple square wave profile model, which must differ substantially from the practical, thick shear layer, case. Nevertheless, several interesting points have been brought out by relating a simple analysis of frequency to one on directivity.

1) Mach waves within the flow do not radiate

2) Observed low frequency components are due to low wave number components in the flow are predicted to radiate at a small angle to the flow.

3) No radiated sound within the flow emerges in the Mach wave direction outside the flow.

4) However, substantial near field noise within the flow is converted to a radiation field near the Mach wave angle outside the flow.

5) Significant high frequency sound radiation would be anticipated at angles somewhat greater than the Mach wave angle.

6) Additional low frequency radiation at a small angle to the jet axis is predicted when $U > a_0 + a_1$.

In addition theoretical predictions of apparent source location have been made for the model.

APPENDIX B

FURTHER EXPERIMENTS

The results discussed in the report have provided much interesting new data on the phonomenon of supersonic jet noise. This data represents only the first part of a comprehensive program which would allow much clearer definition of the noise field. This Appendix presents recommendations for further experiments which are required to follow up the present phase of the work. In part these recommendations follow the original experimental plan presented in Reference 30. The most important requirement is for acoustic measurements which will allow correlation of the observed shadowgraph field with recorded sound levels. From the present work it is clear that additional tests on hot jets are required, and it is recommended that all tests be re-run at the maximum possible stagnation temperature (500°F in the present facility). In addition several experiments to define the mechanisms underlying the observed noise field are recommended.

In summary the recommended experimental program requires:

(1) Set up acoustic instrumentation (Reference 33)

(2) Perform combined shadowgraph and far field acoustic measurements for high stagnation temperature jet in various over and under expanded cases.

(3) Perform simultaneous normal and oblique shadowgraphs on fully expanded jet

(4) If successful, simultaneous shadowgraphs will be taken of all expansion cases

(5) Design and construct screens for double exposure shadowgraphs (Reference 30)

(6) Set up screens and study fully expanded jet using double exposure shadowgraphs at various time delays

(7) If justified, study other cases

(8) Check correlation ofpeaks in near field microphone output with Mach waves

(9) If successful, record time histories of sound pressure at a group of three microphones, possibly with simultaneous shadowgraphs. Number of cases studied to be decided at future date, but limited initially to fully expanded case.

(10) Analyze time histories to give position and strength of Mach wave sources

(11) Construct and set up instrumented deflector plate (Reference 30)

(12) Run hot deflected jet tests, and record deflector surface pressures and sound radiation

(13) Analyze sound pressures for all runs, and deflector surface pressures, to give level and spectrum (1/3 octave)

(14) Analyze and interpret results

Additional details of the proposed work and sketches of the various rigs required may be found in References 30 and 33. It is anticipated that completion of the tests recommended here would provide much new knowledge, and suggest several improvements for the prediction and control of noise from rocket exhaust flows.

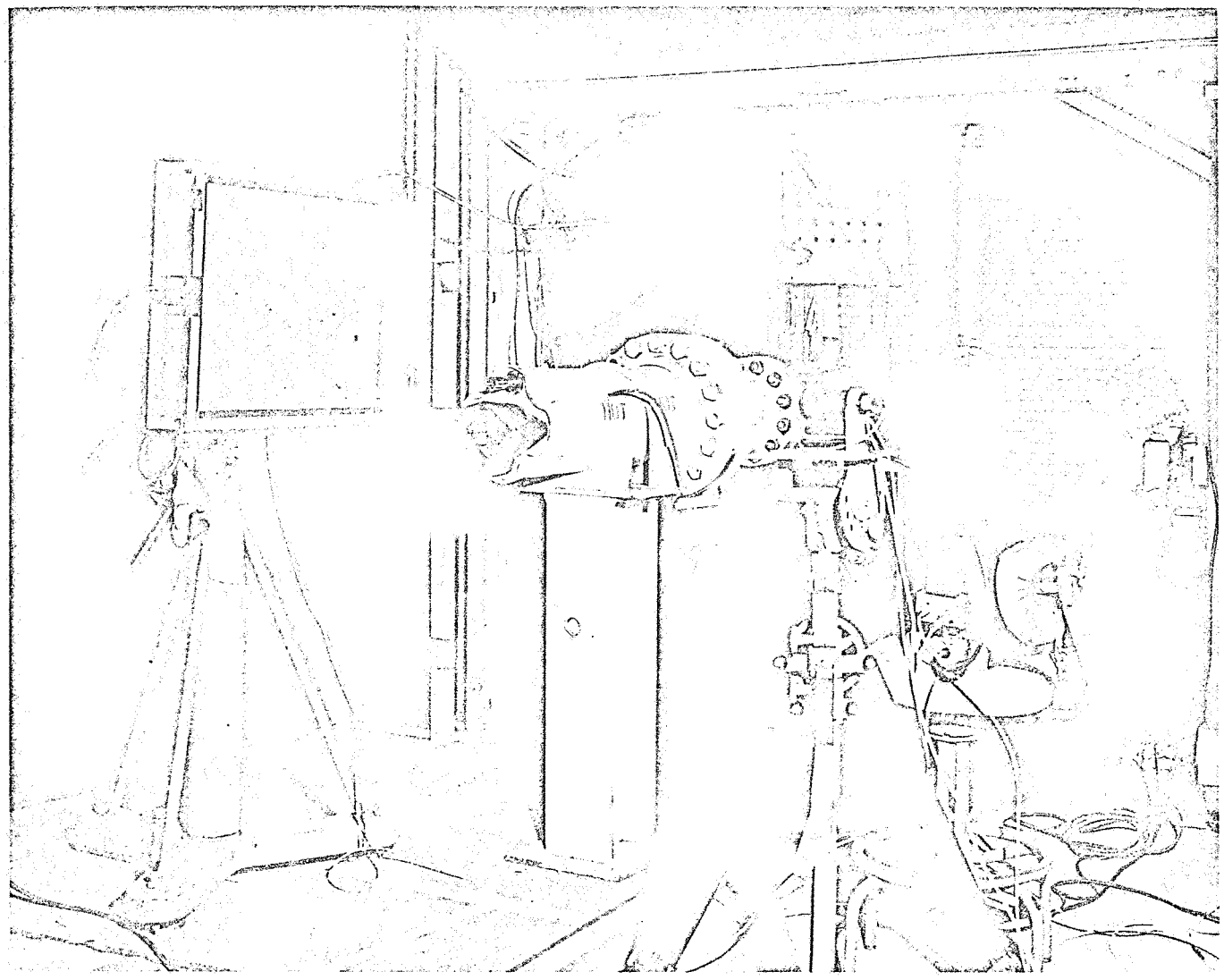

Figure 1. Experimental Arrangement for Undeflected Jets

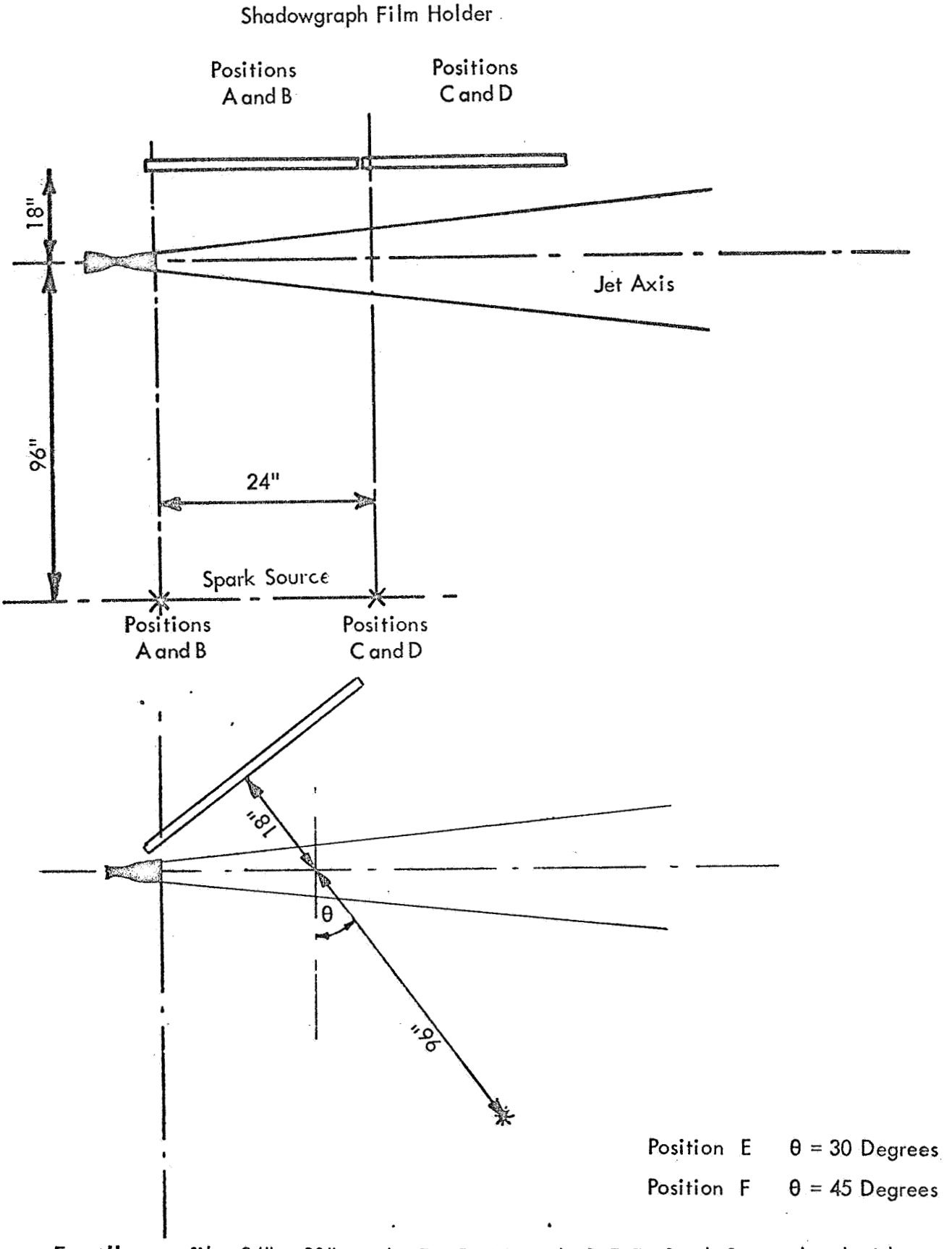

For all cases film 24" x 20" used. For Positions A,C,E,F, Spark Source level with Jet, shadowgraph bottom edge is approximately 1.5 inches below Jet. Positions B and D, Spark Source 20" above axis, shadowgraph bottom edge approximately 18.5 inches above Jet Axis.

Figure 2. Dimensions for Undeflected Jet Tests

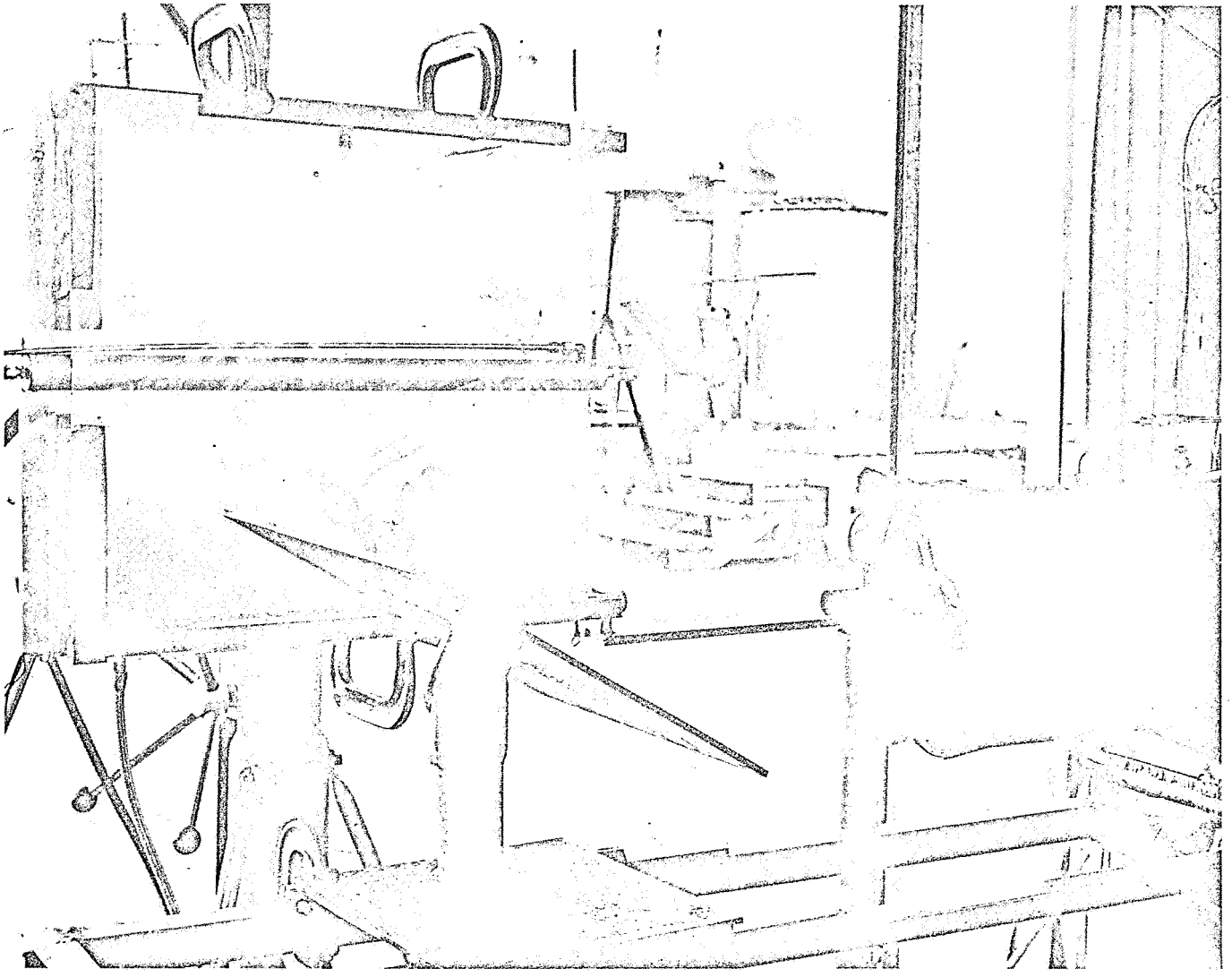

Figure 3. Experimental Arrangement for Deflected Jets

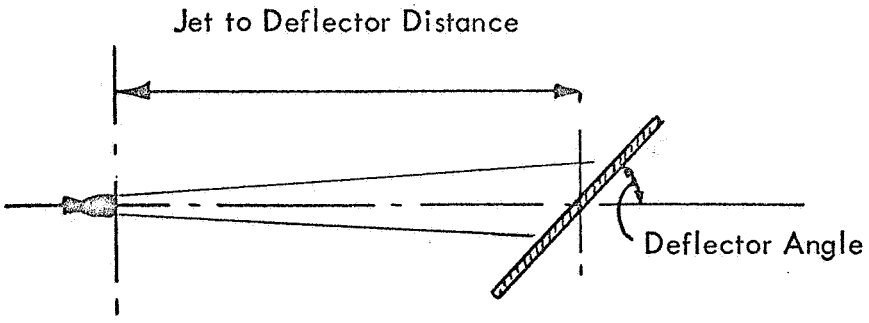

Deflector Plate is 16 Inches Square, and Placed with Center on Jet Axis.

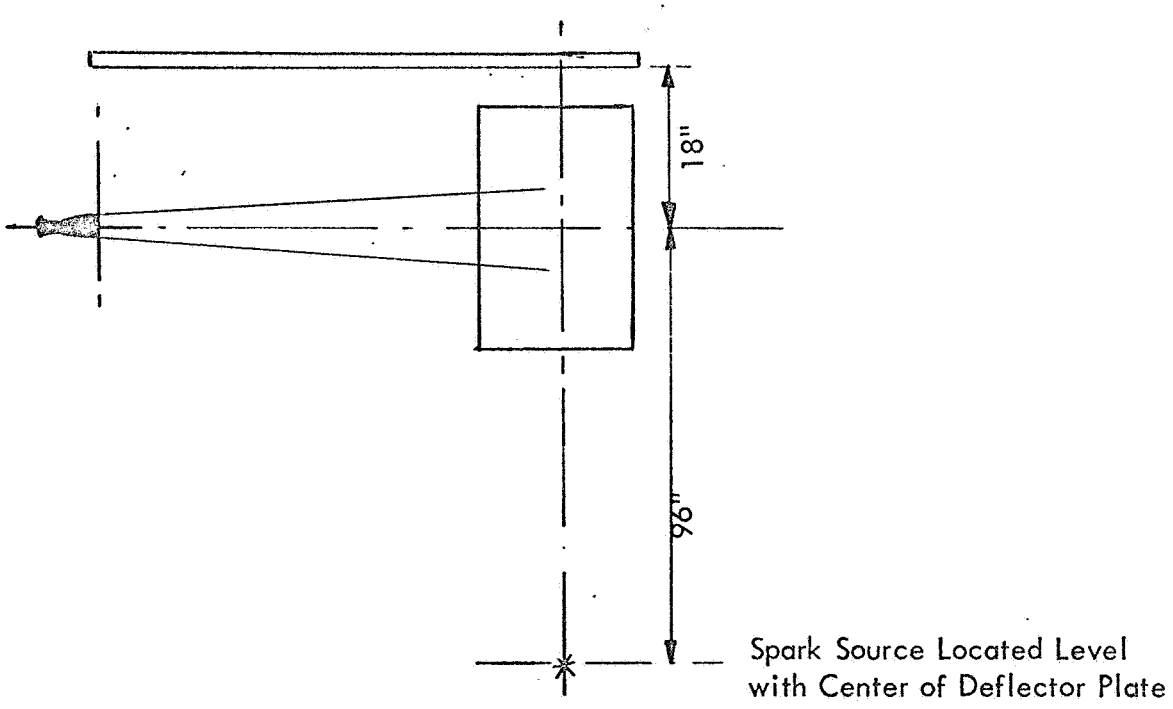

Figure 4. Dimensions for Deflected Jet Tests.

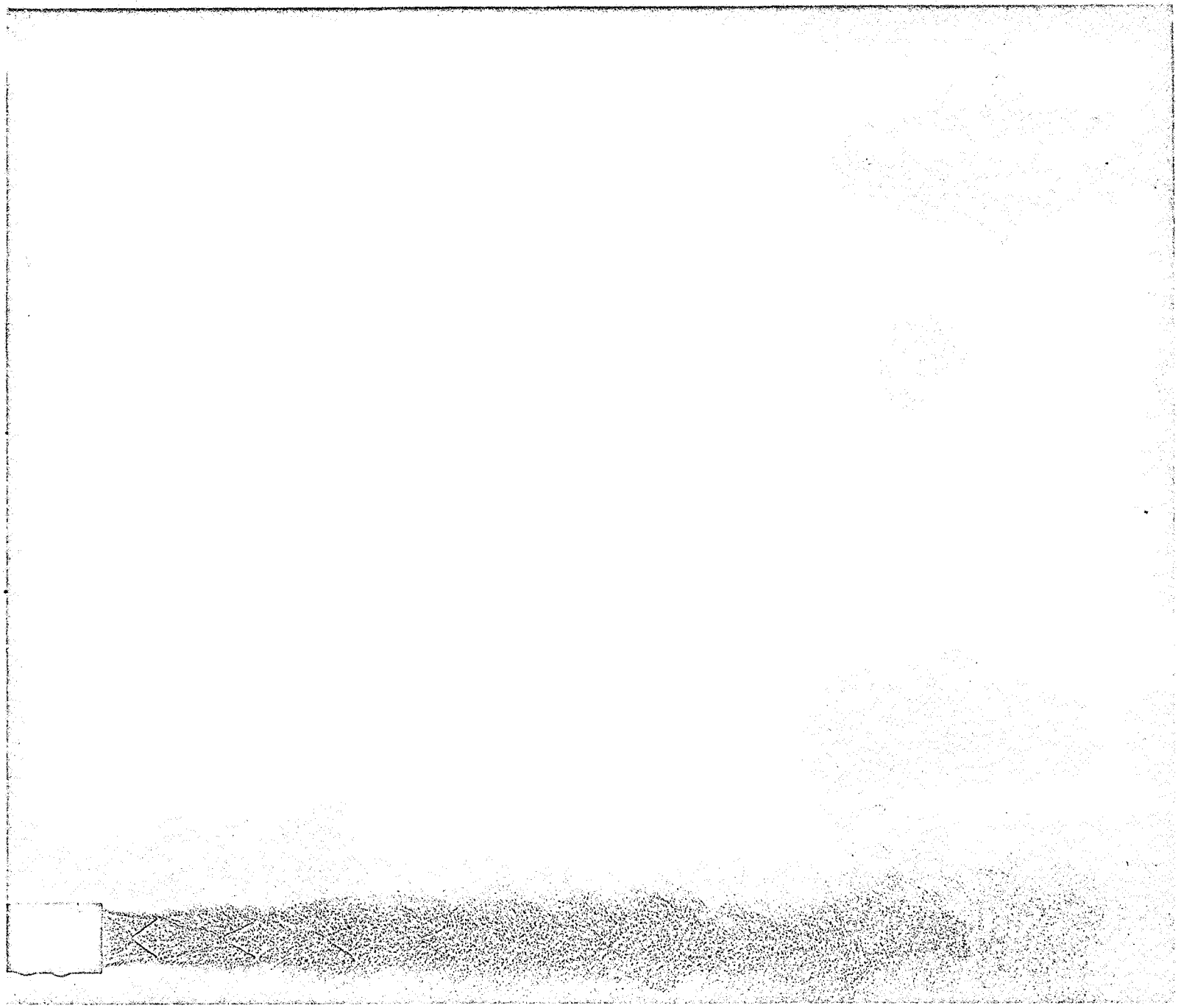

Figure 5. Undeflected Jet at 50 Percent Ideal Pressure

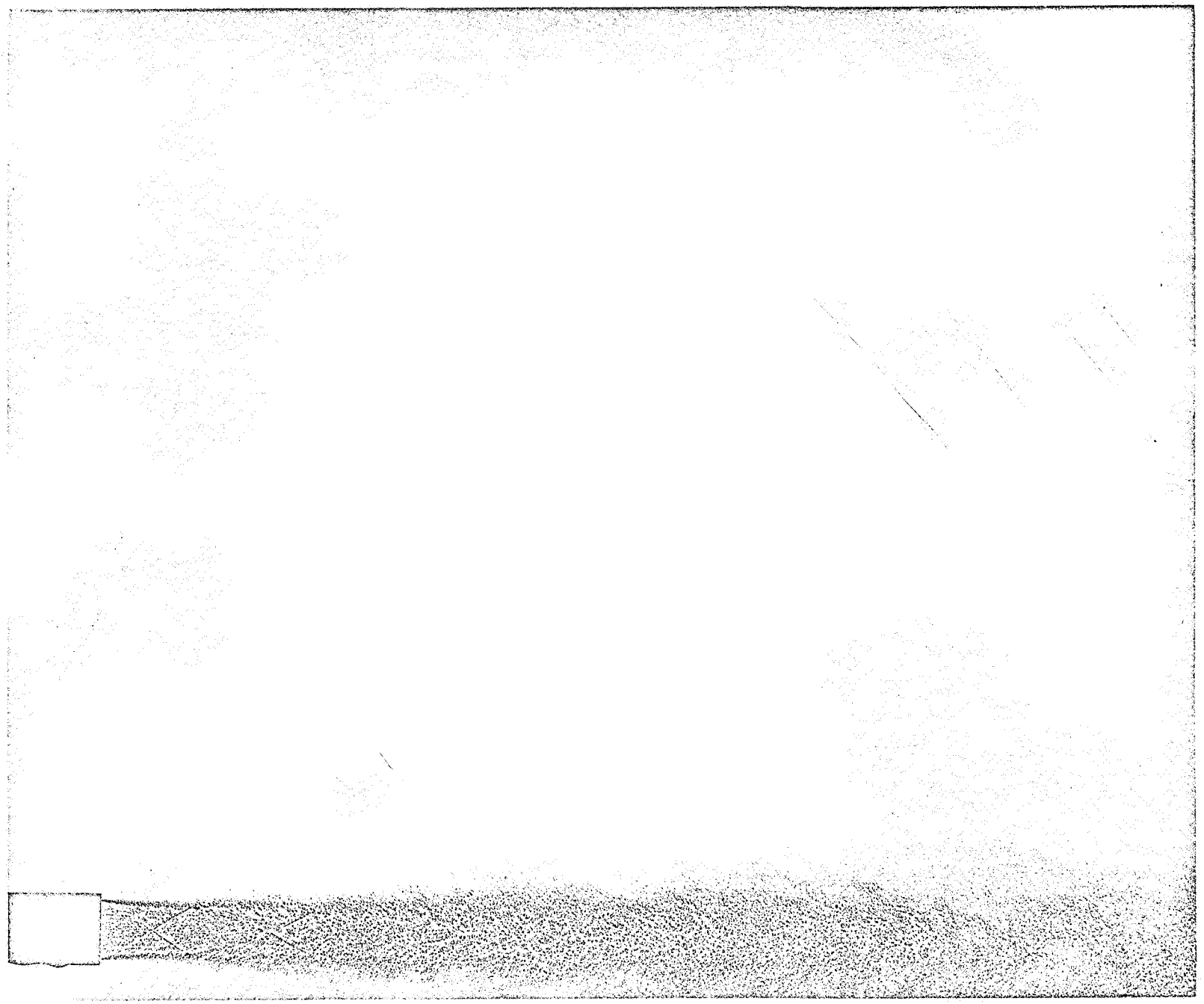

Figure 6. Undeflected Jet at 75 Percent Ideal Pressure

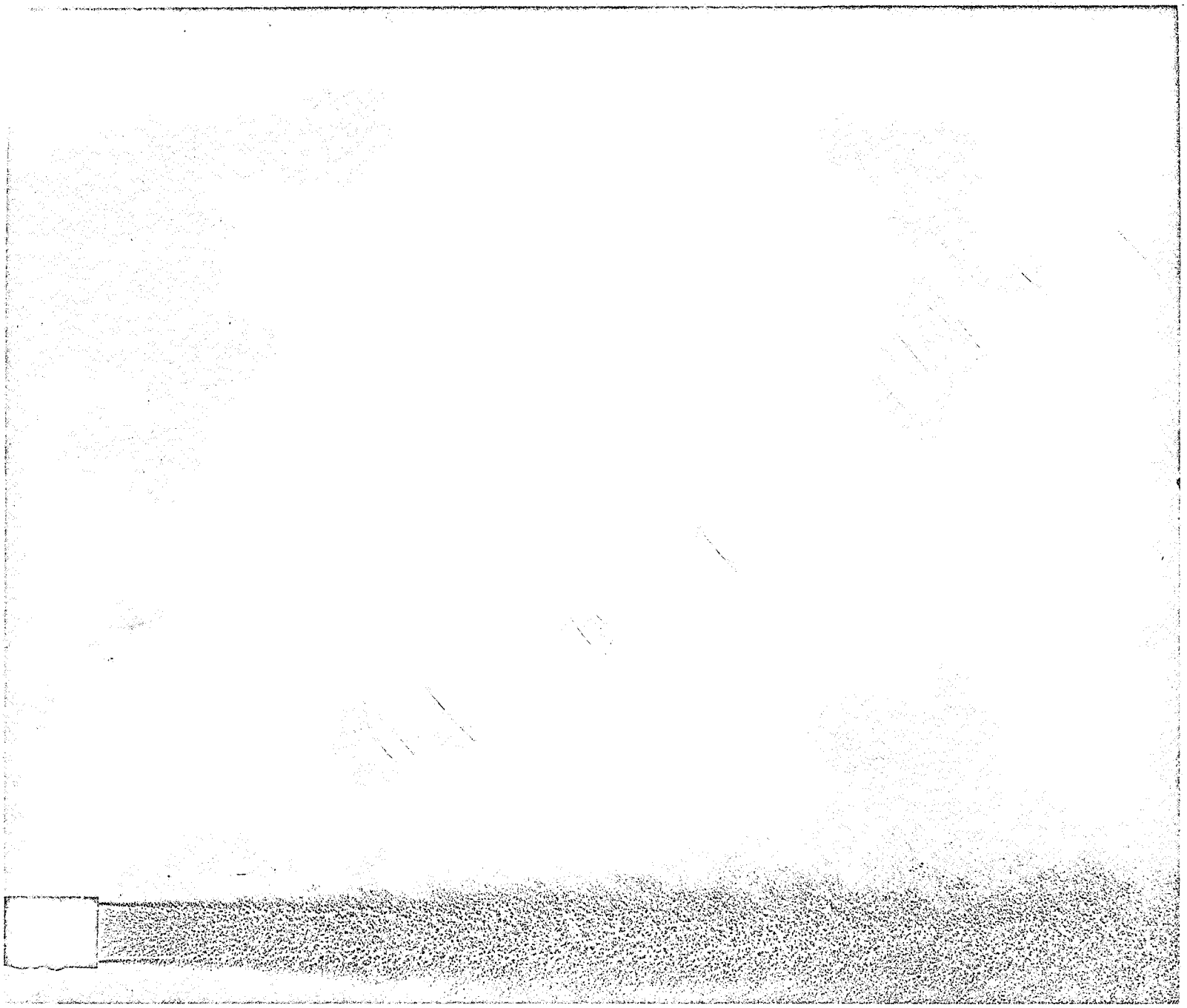

Figure 7. Undeflected Jet at 100 Percent Ideal Pressure

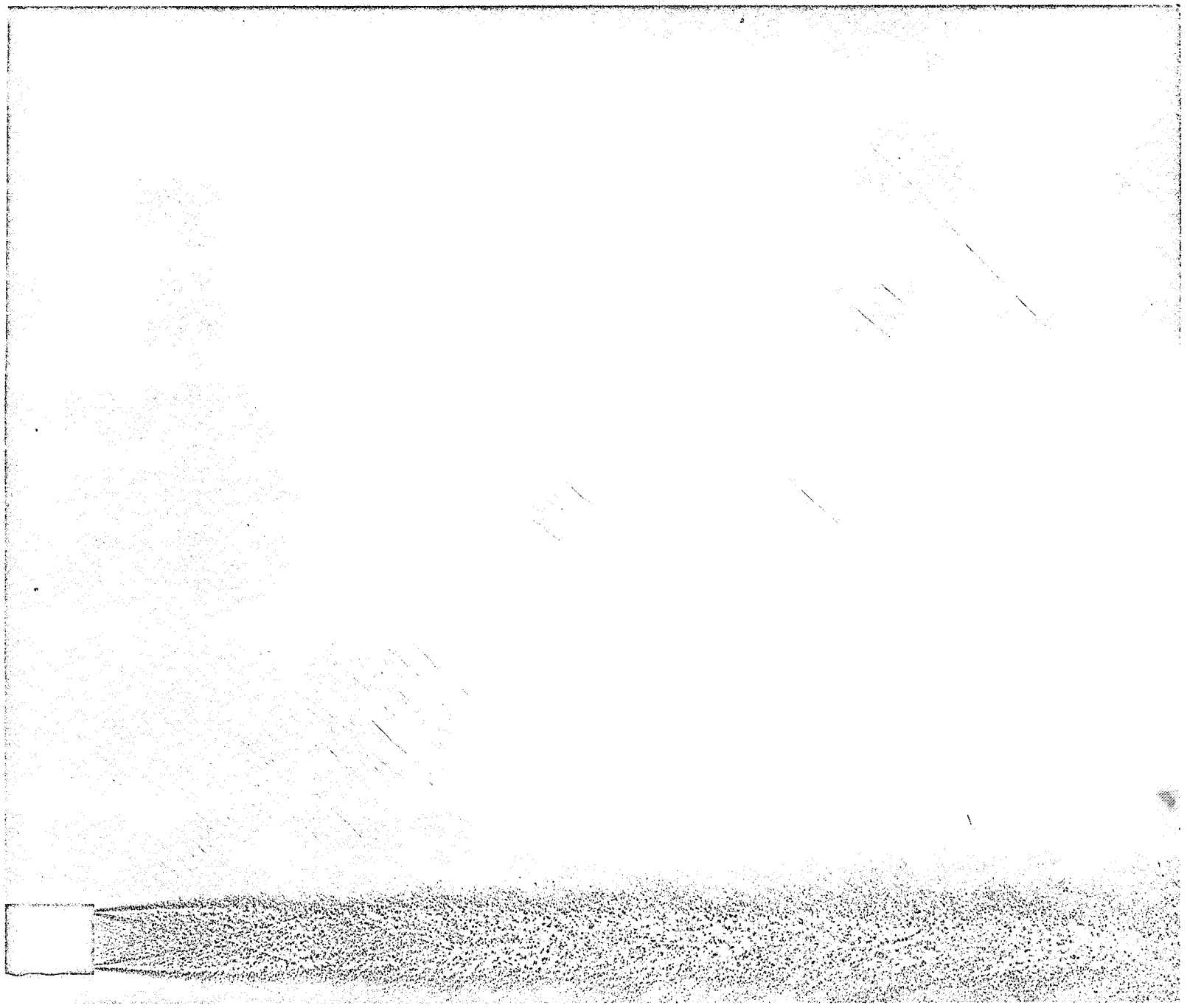

Figure 8. Undeflected Jet at 153 Percent Ideal Pressure

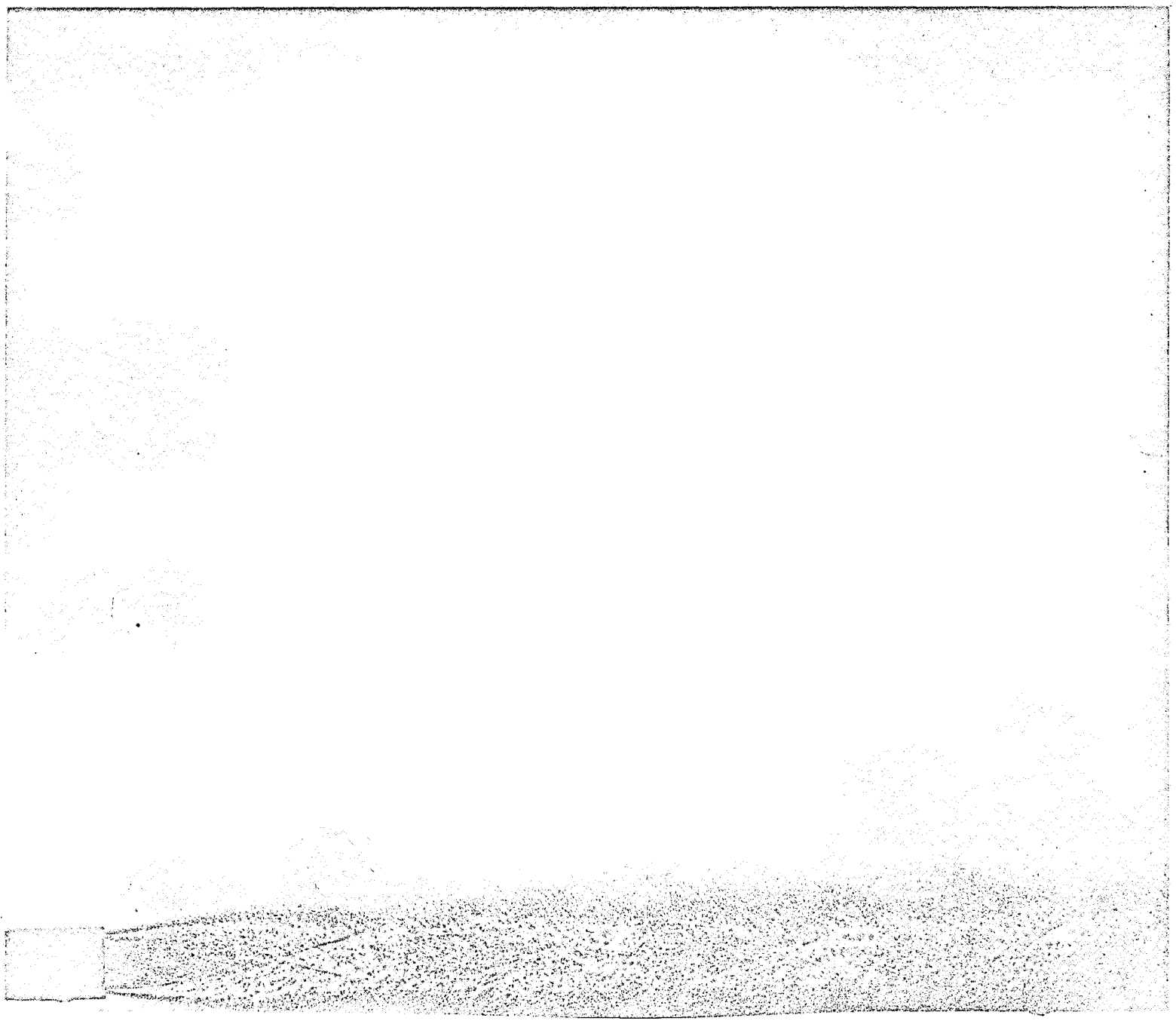

Figure 9. Undeflected Jet at 198 Percent Ideal Pressure

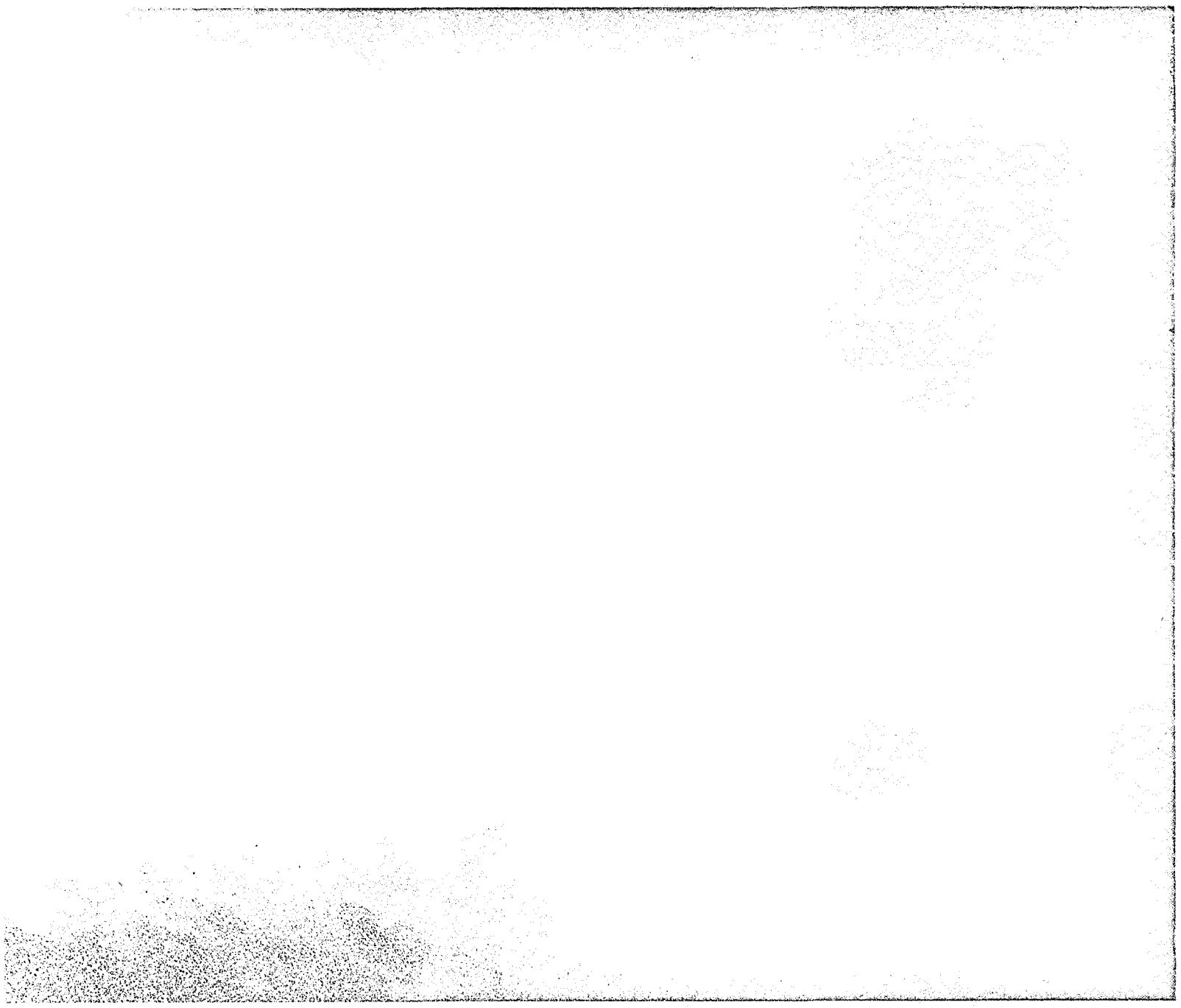

Figure 10. Undeflected Jet at 100 Percent Ideal Pressure - Position D

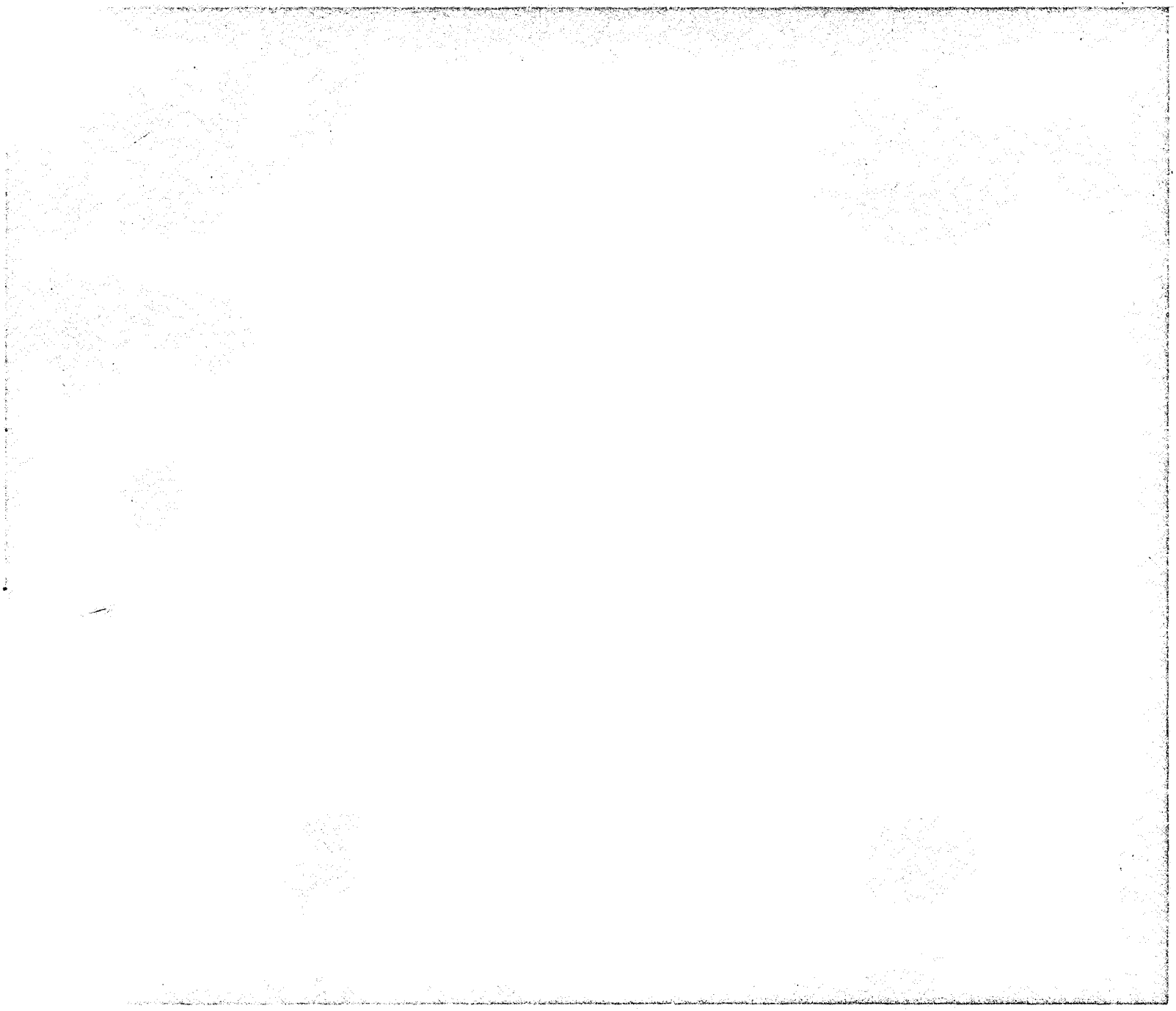

Figure 11. Undeflected Jet at 100 Percent Ideal Pressure - Position C

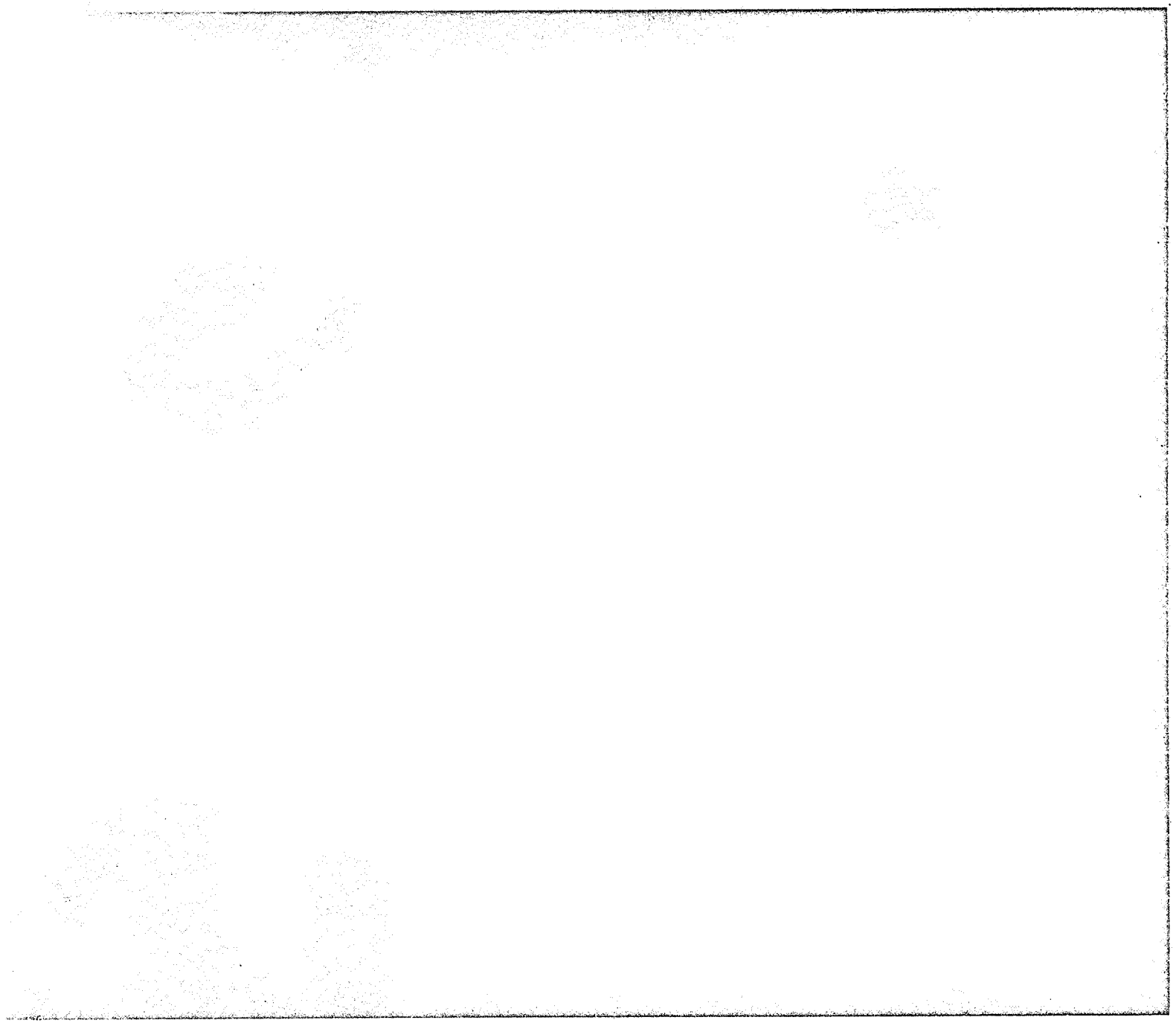

Figure 12. Undeflected Jet at 100 Percent Ideal Pressure - Position B

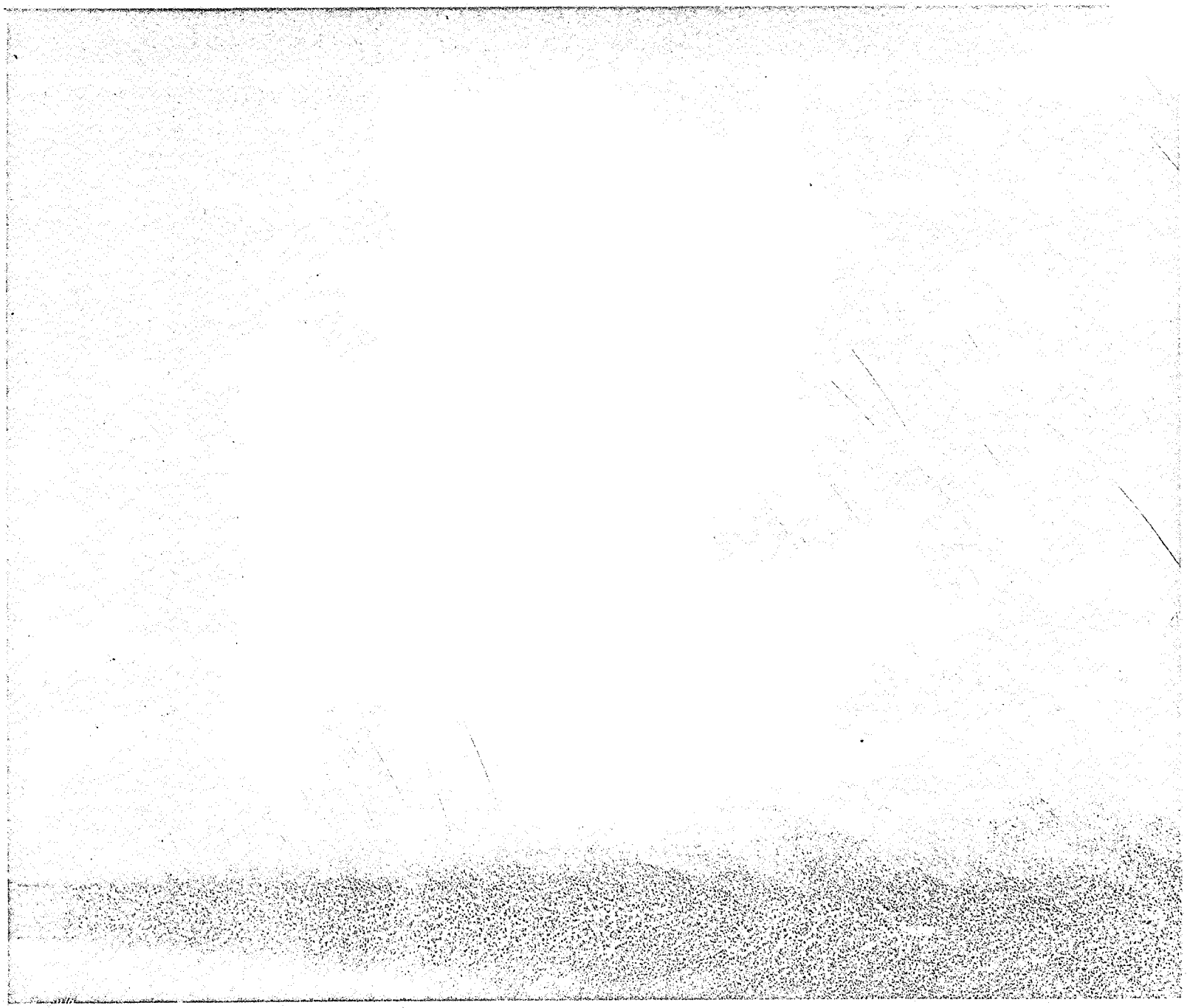

Figure 13. Undeflected Jet at 100 Percent Ideal Pressure - Position E (30 Degree Oblique)

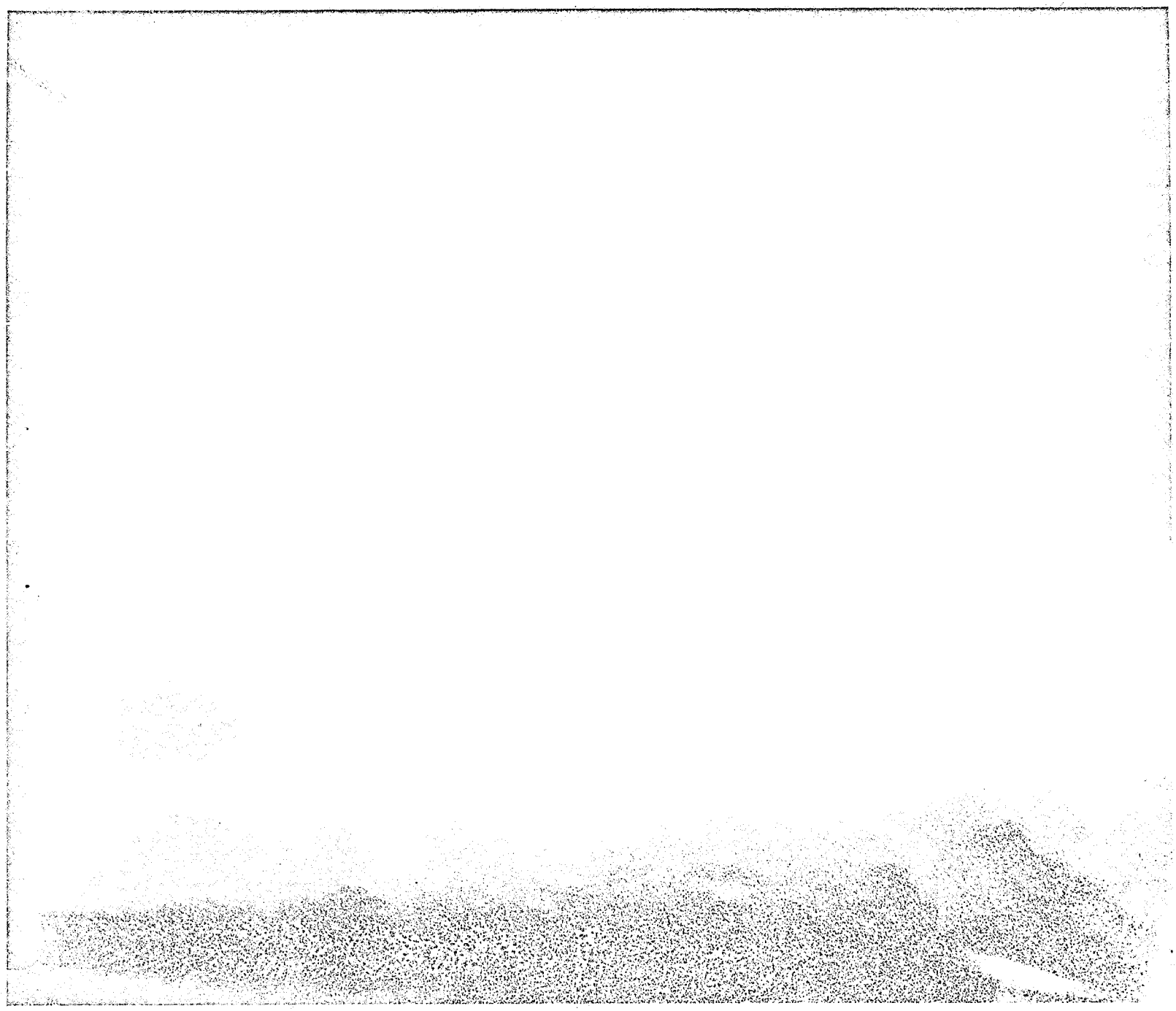

Figure 14. Undeflected Jet at 100 Percent Ideal Pressure - Position F (45 Degree Oblique)

Figure 15. Deflected Jet at 100 Percent Ideal Pressure, Jet to Deflector Distance 4.25 inches

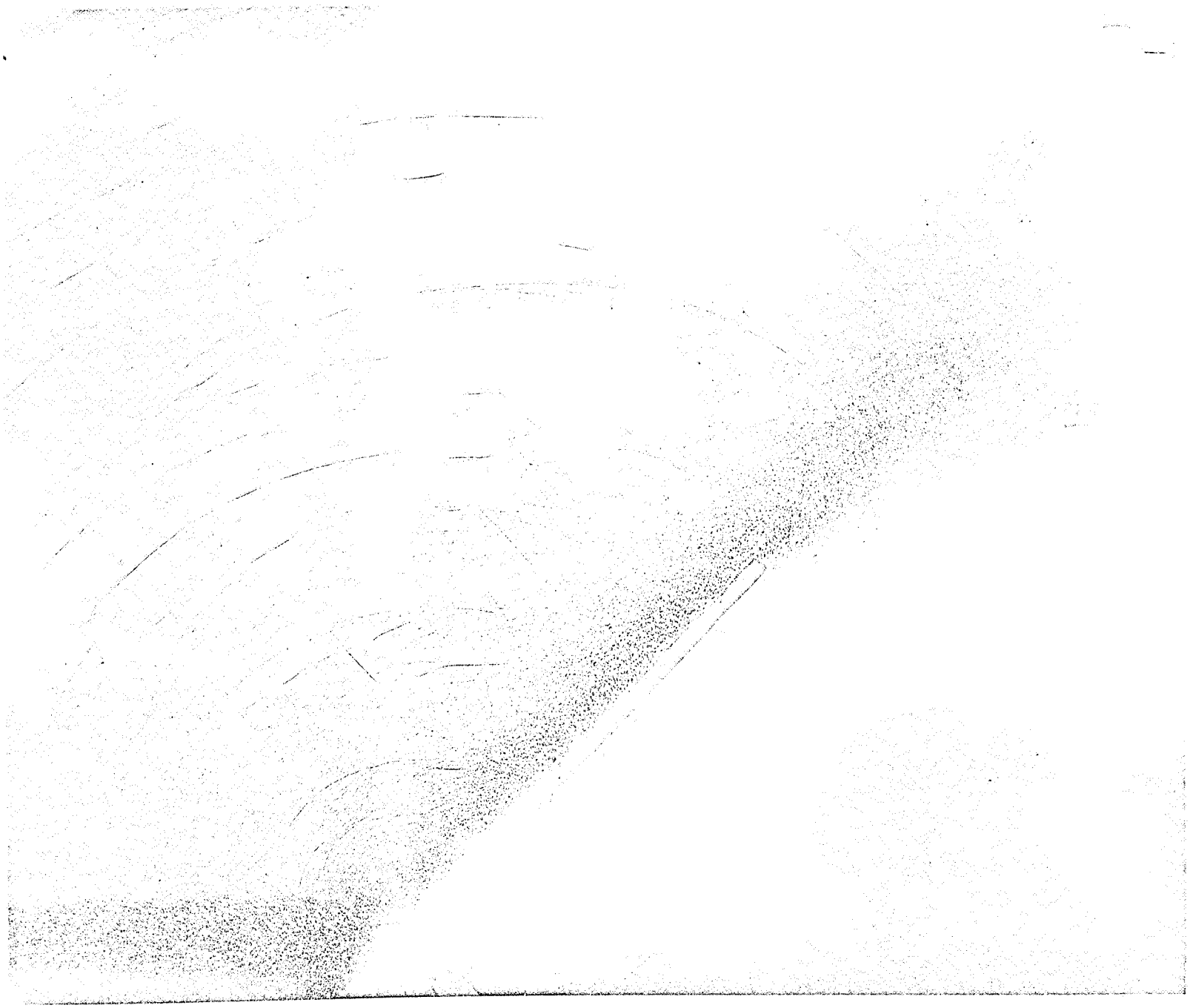

Figure 16. Deflected Jet at 100 Percent Ideal Pressure, Jet to Deflector Distance 8.0 inches

Figure 17. Deflected Jet at 157 Percent Ideal Pressure, Jet to Deflector Distance 8.0 inches

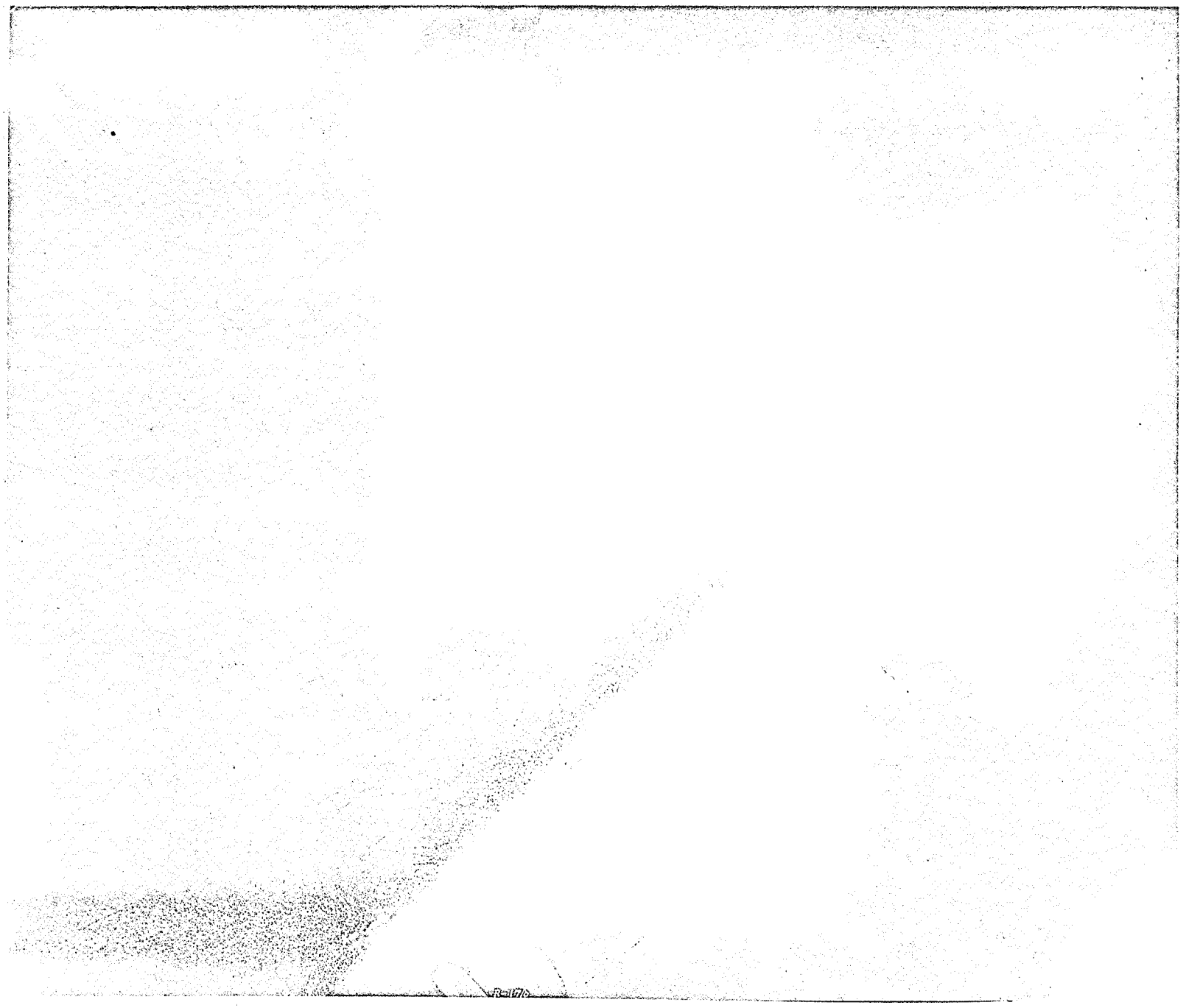

Figure 18. Deflected Jet at 76 Percent Ideal Pressure, Jet to Deflector Distance 8.0 inches

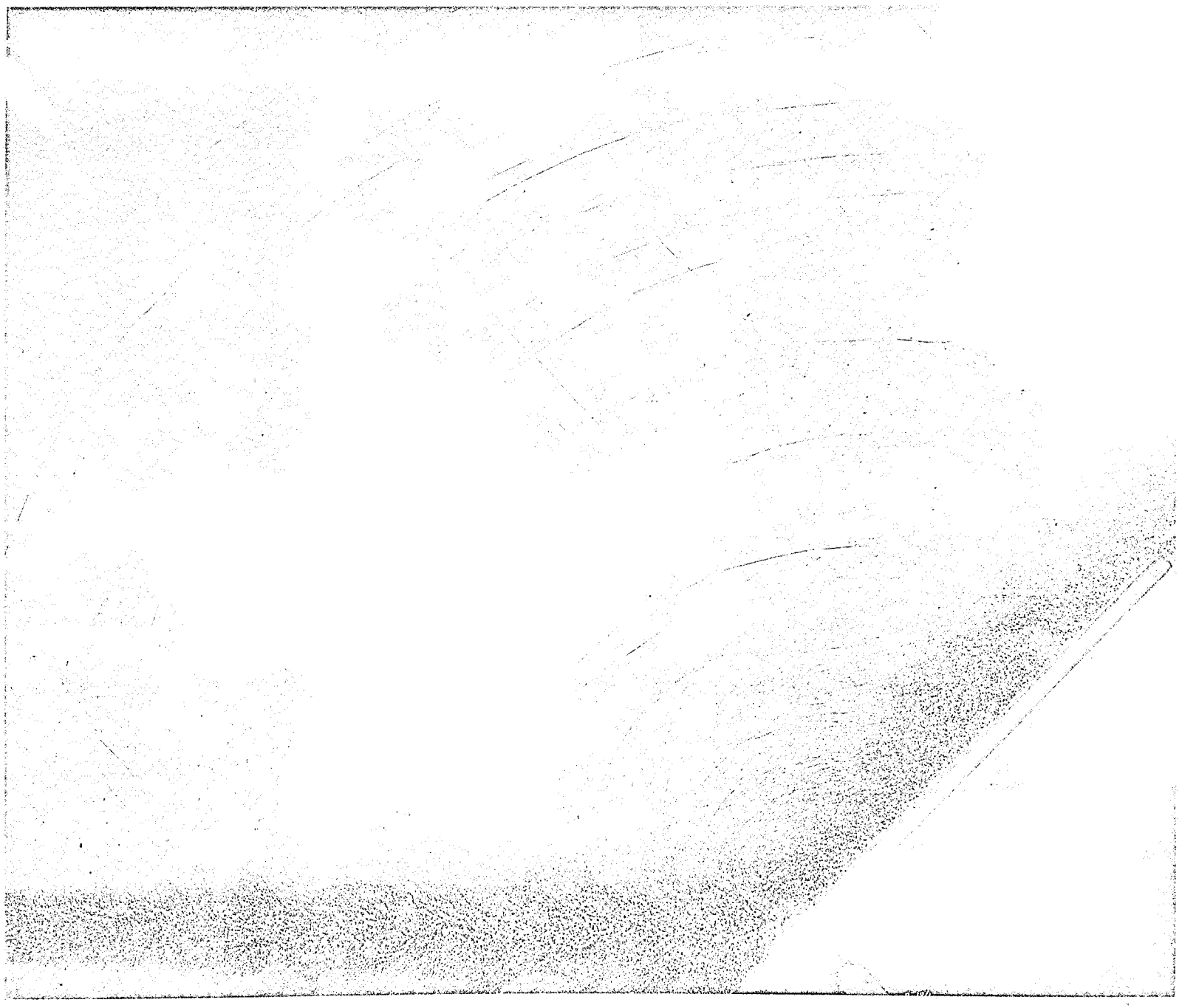

Figure 19. Deflected Jet at 100 Percent Ideal Pressure, Jet to Deflector Distance 16.0 inches

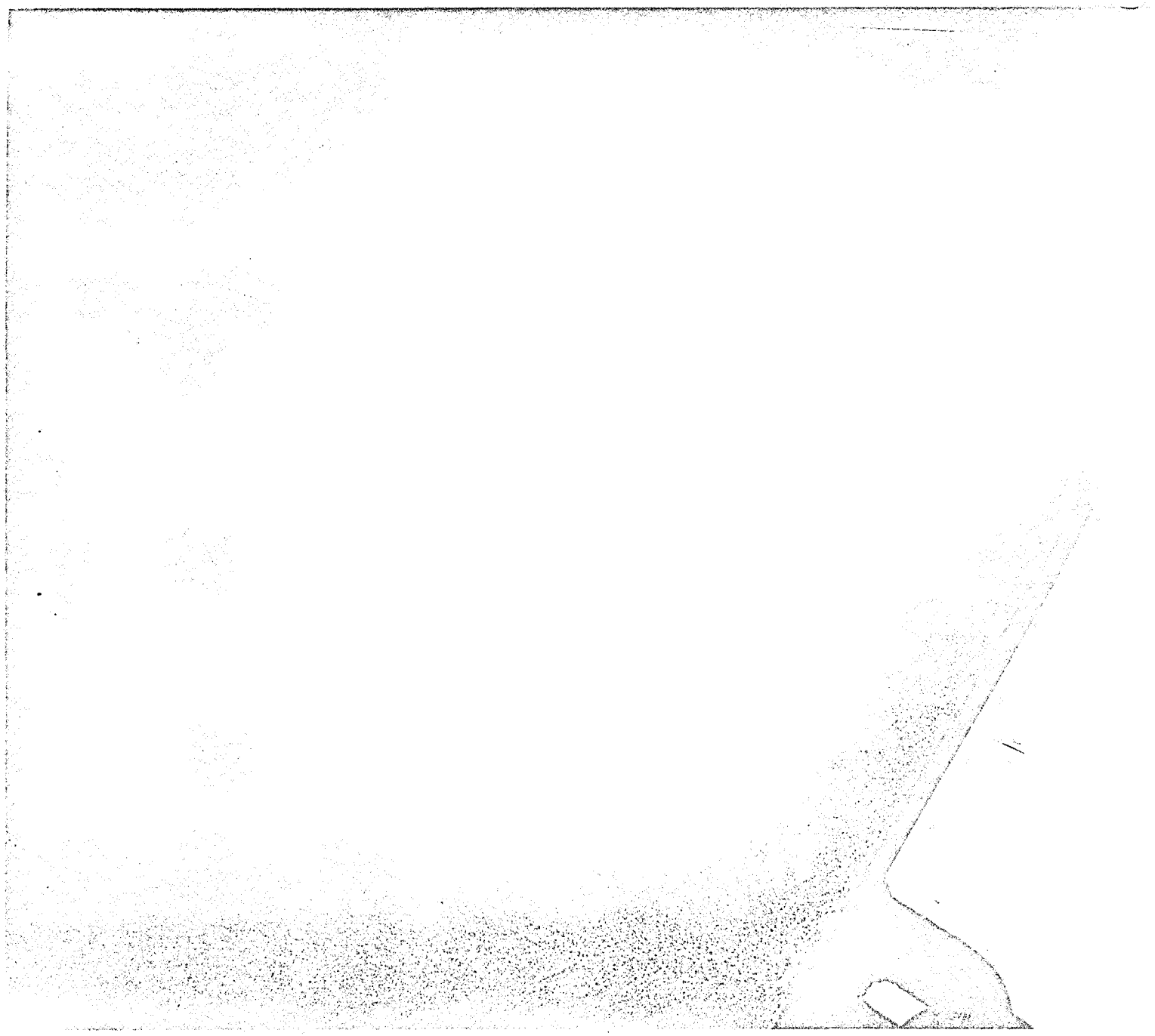

Figure 20. Deflected Jet at 100 Percent Ideal Pressure, Jet to Deflector Distance 16.0 inches Deflector Angle = 60 Degrees

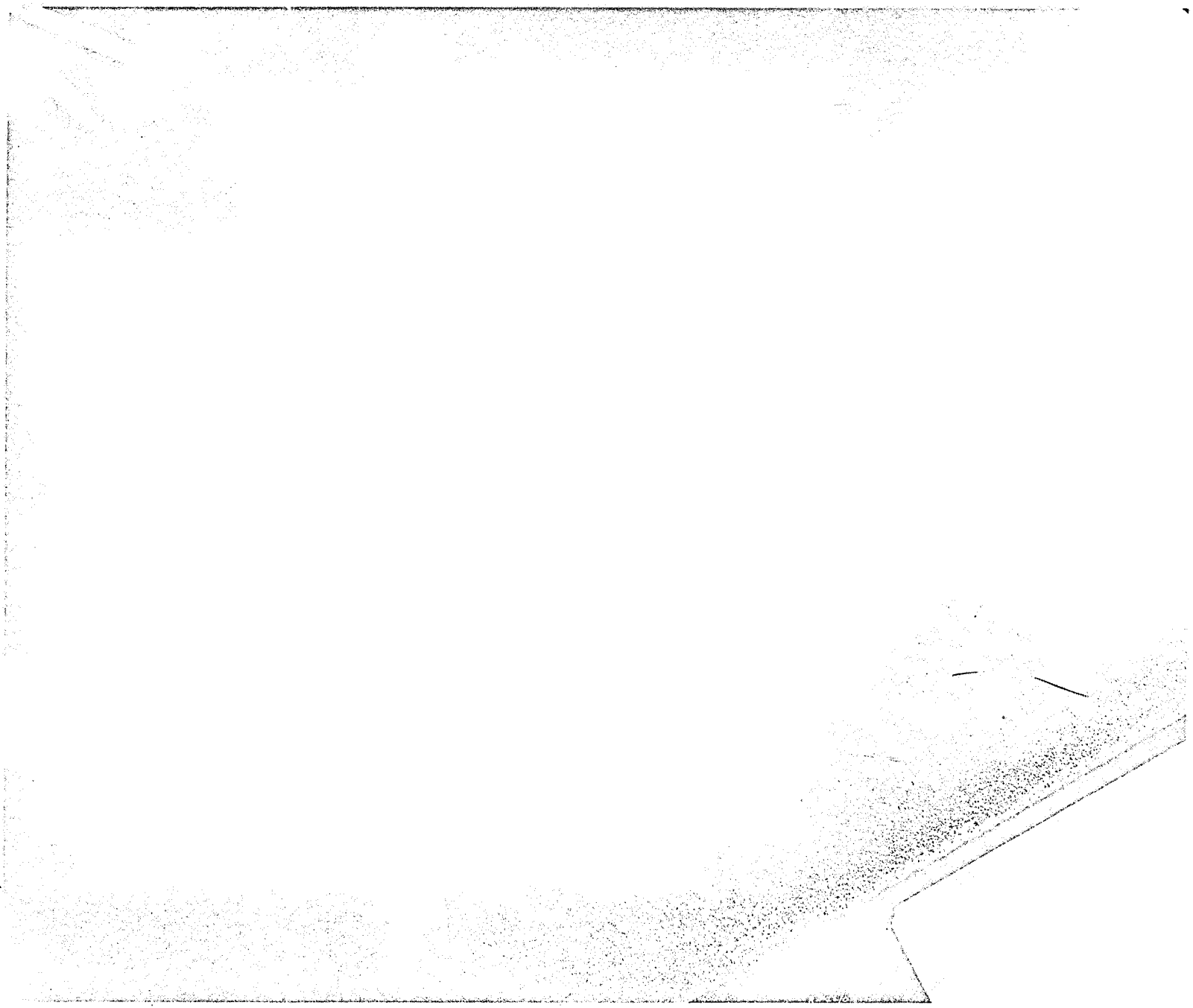

Figure 21. Deflected Jet at 100 Percent Ideal Pressure, Jet to Deflector Distance 16.0 inches
Deflector Angle = 30 Degrees

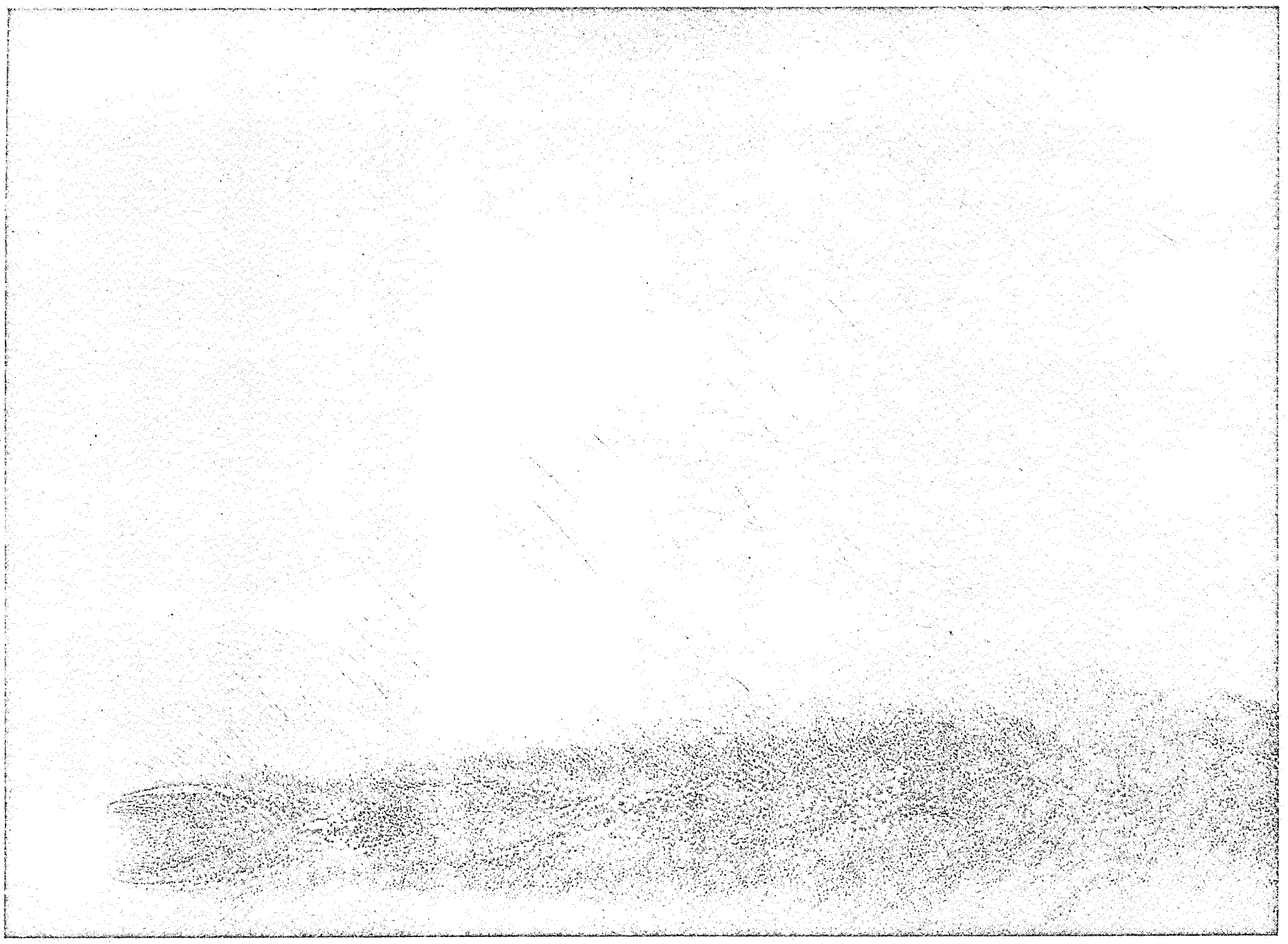

Figure 22. Flow From Conical Nozzle

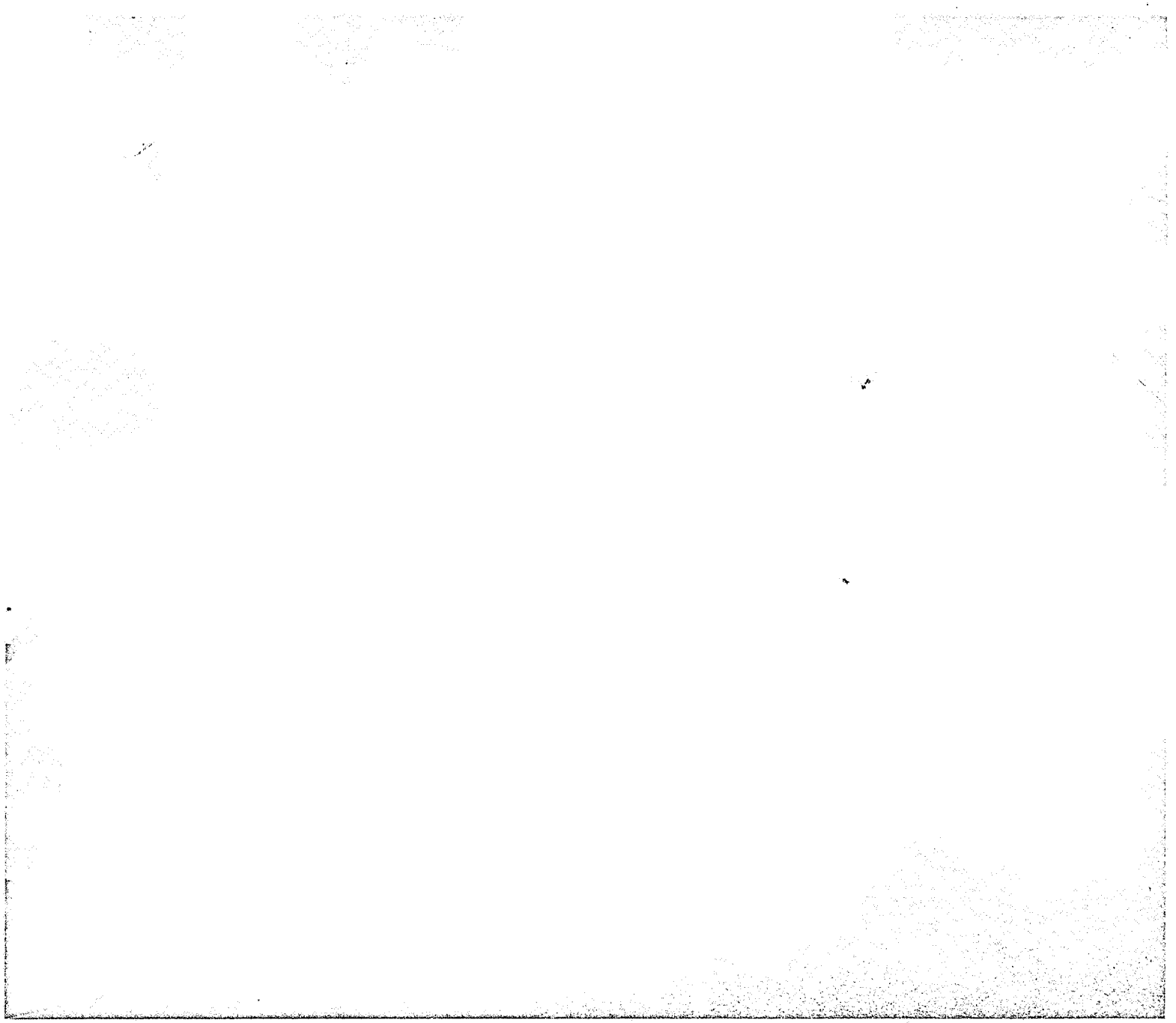

Figure 23. Ideally Expanded Flow at 300°F Stagnation Temperature (Result from Langley Research Center)

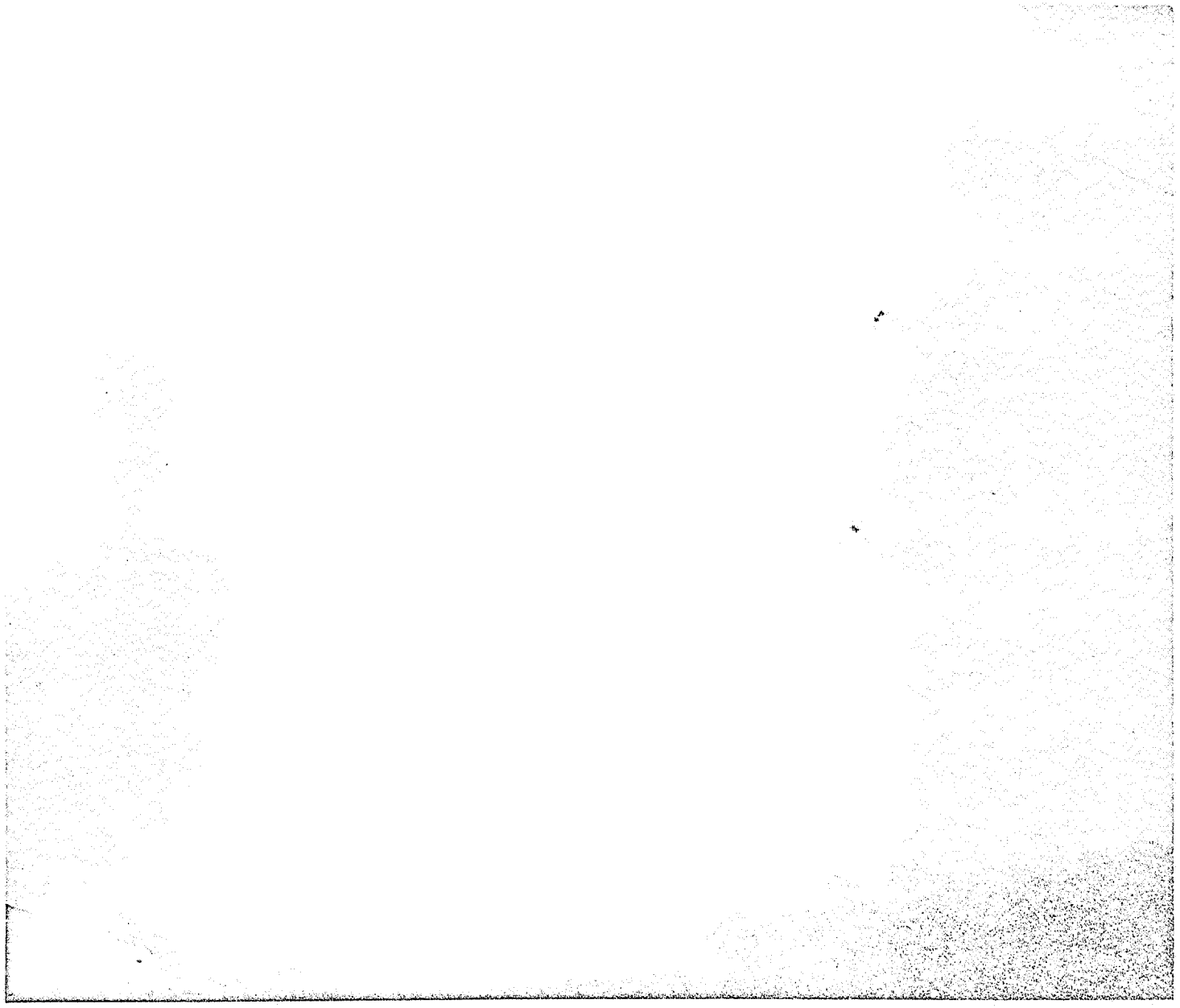

Figure 24. Ideally Expanded Flow at 1200°F Stagnation Temperature (Result from Langley Research Center)

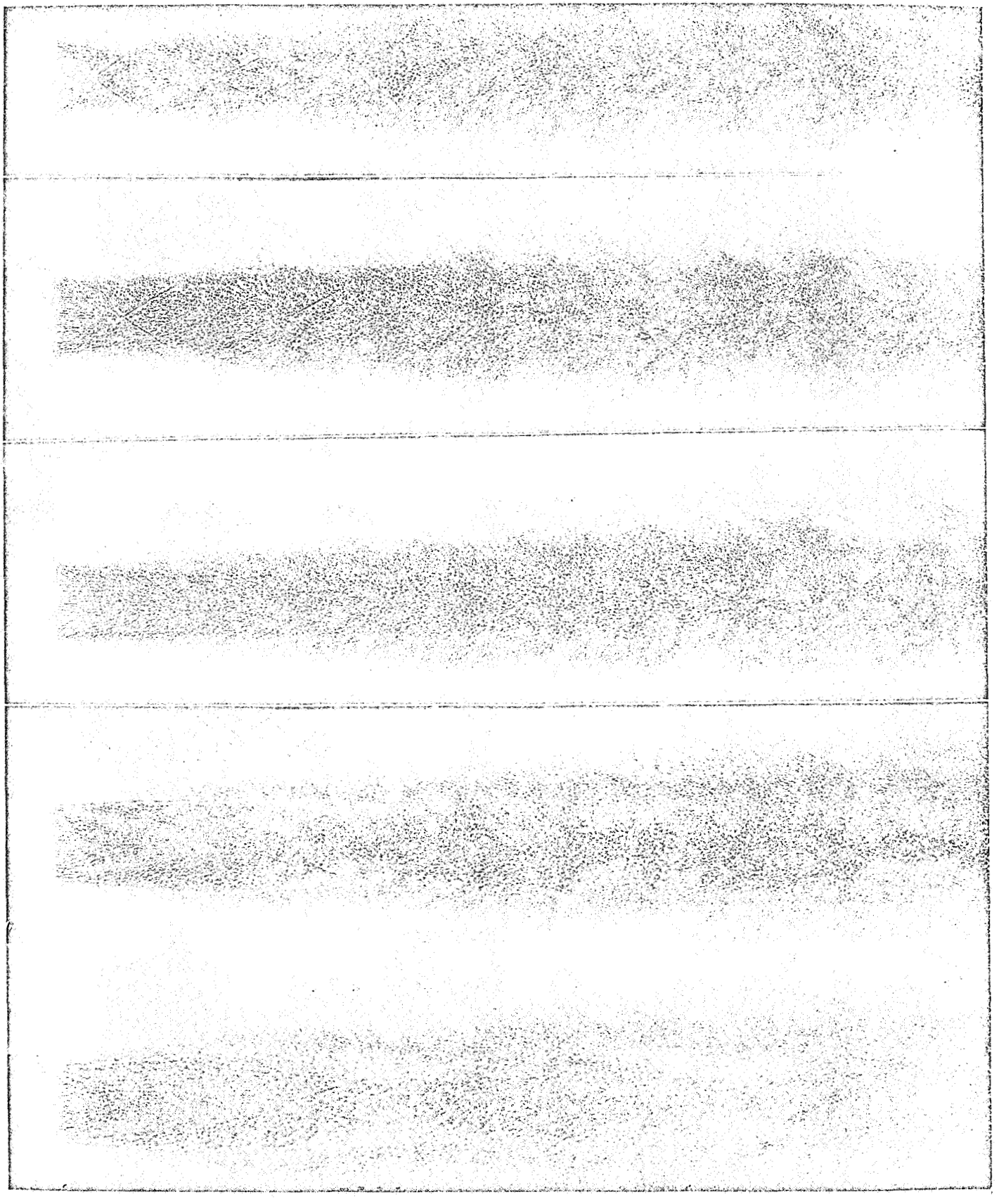

Figure 25. Comparison of Flow at Various Expansion Ratios

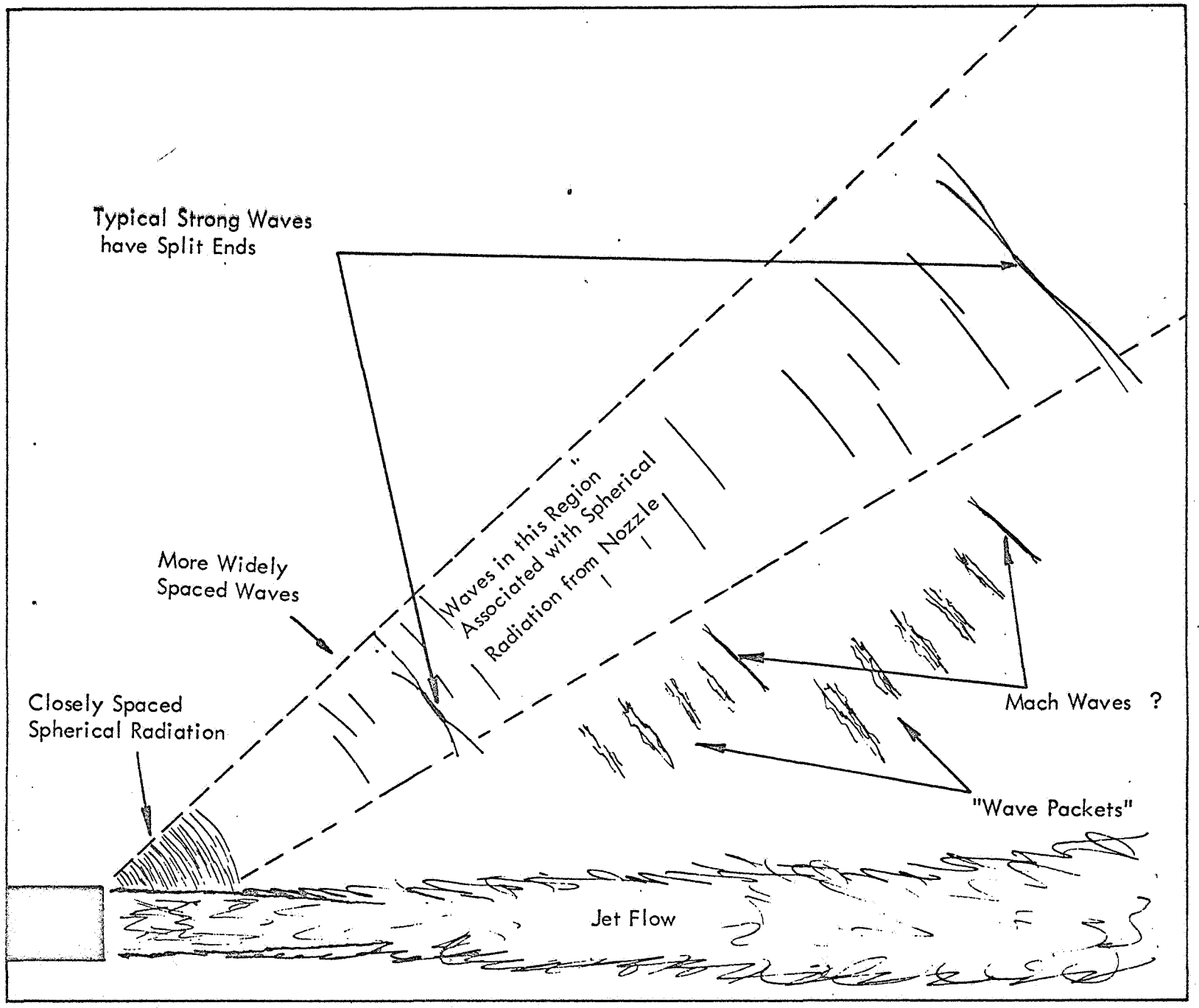

Figure 26. Diagram Showing Features of Flow in Figure 7.

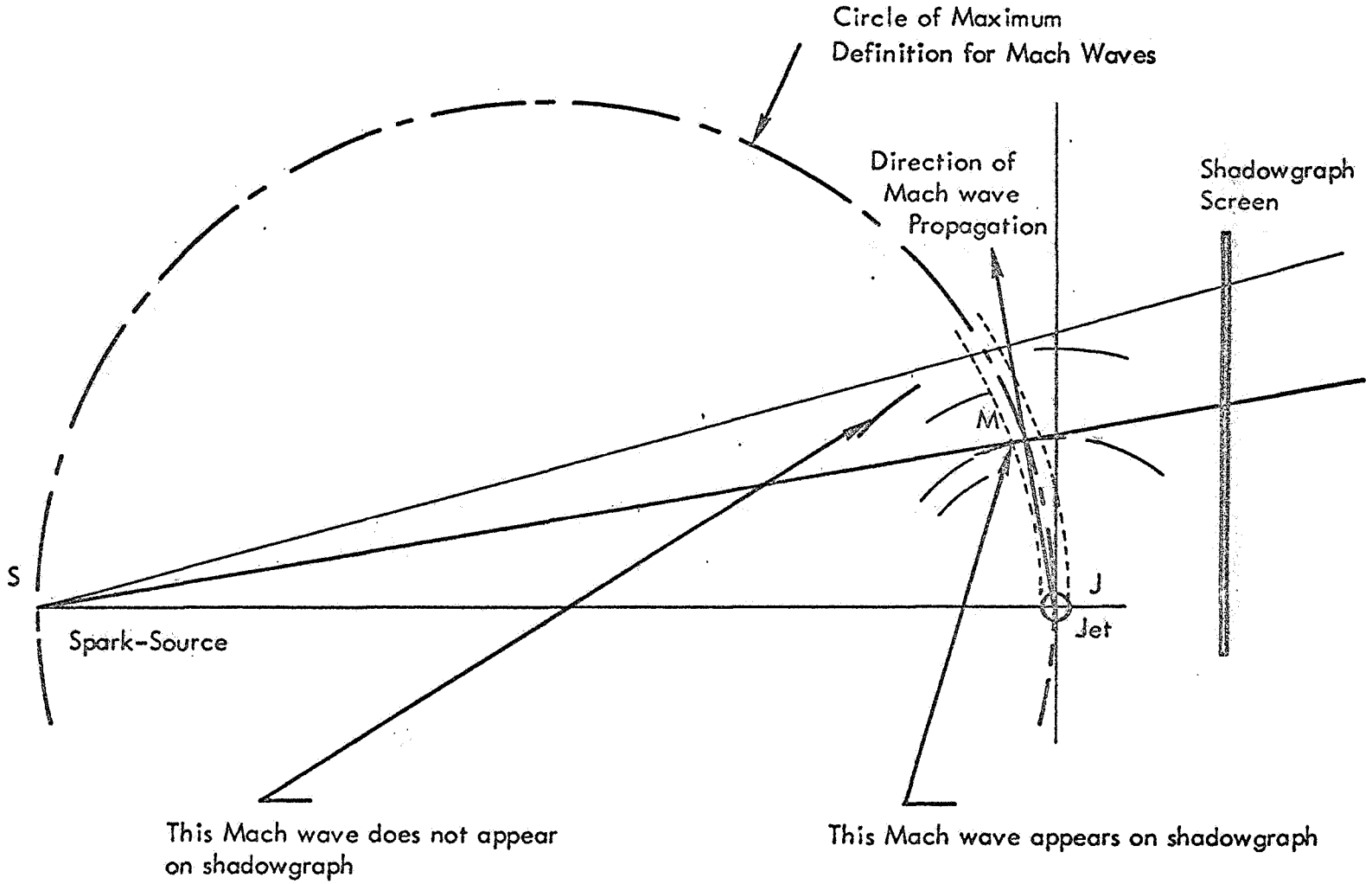

Figure 27. Details of Shadowgraph Photography of Mach Waves

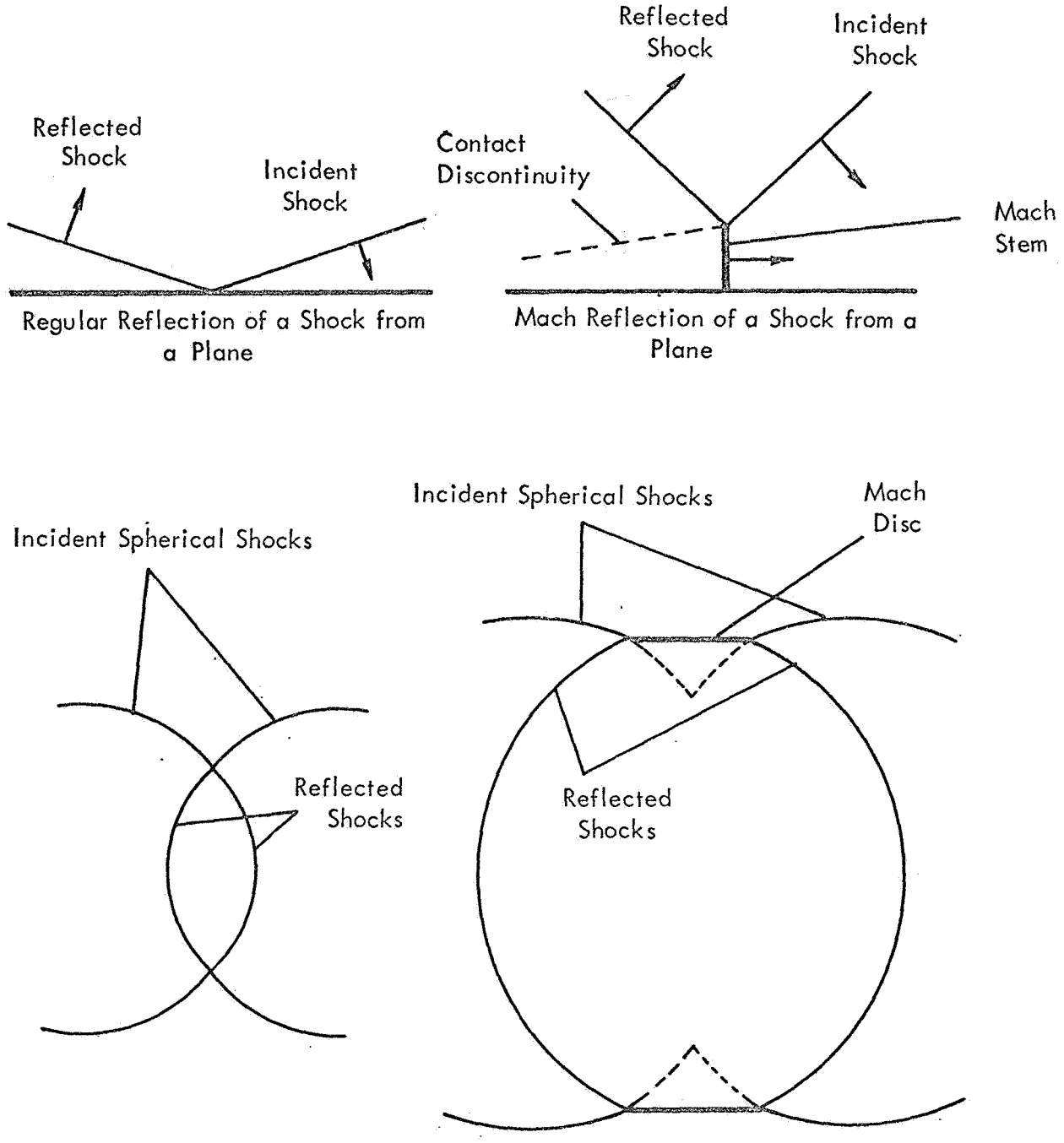

Figure 28. Regular and Mach Reflection for a Plane and Spherical Wave

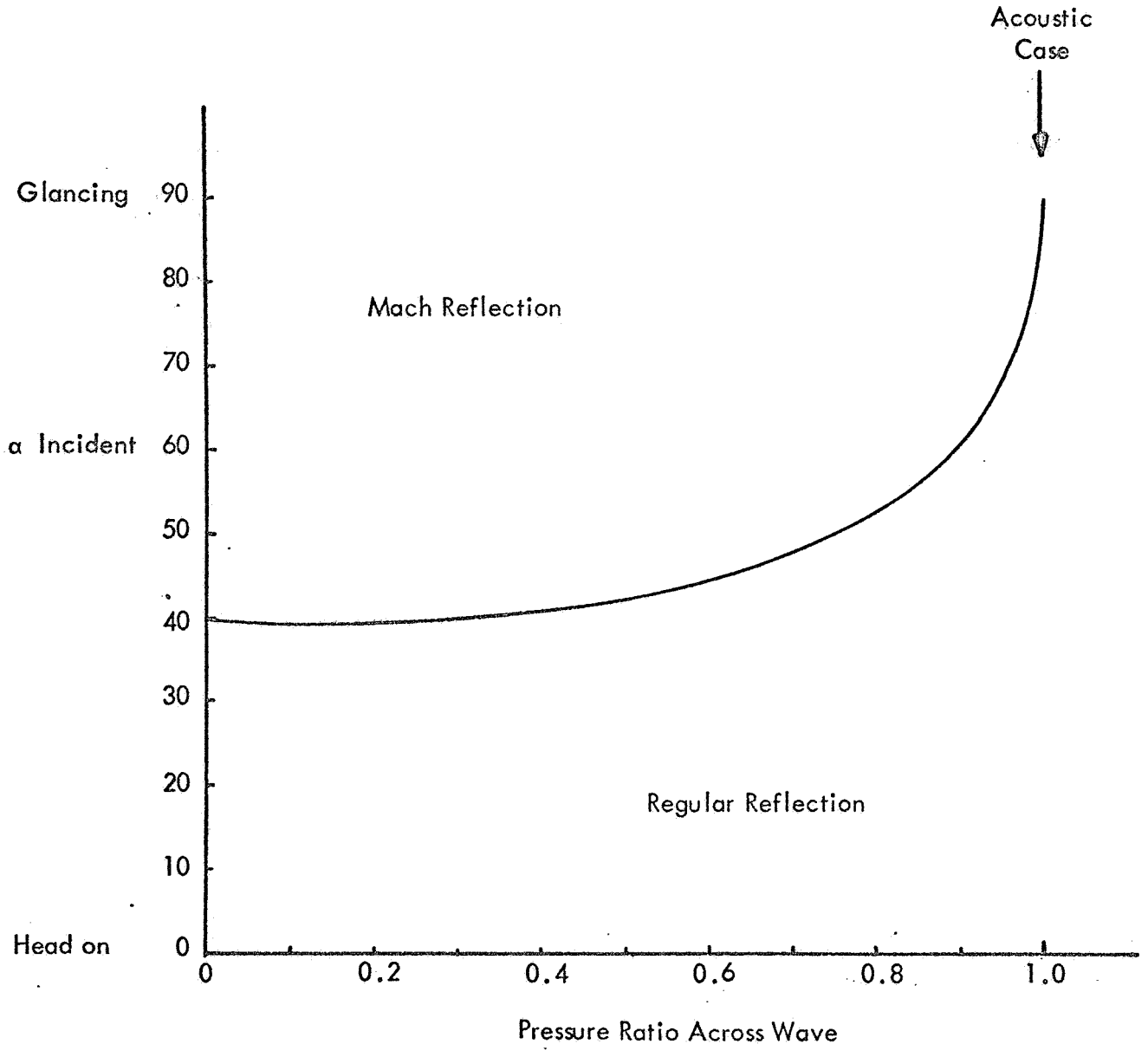

Figure 29. Theoretical Limiting Angle for Mach Reflection

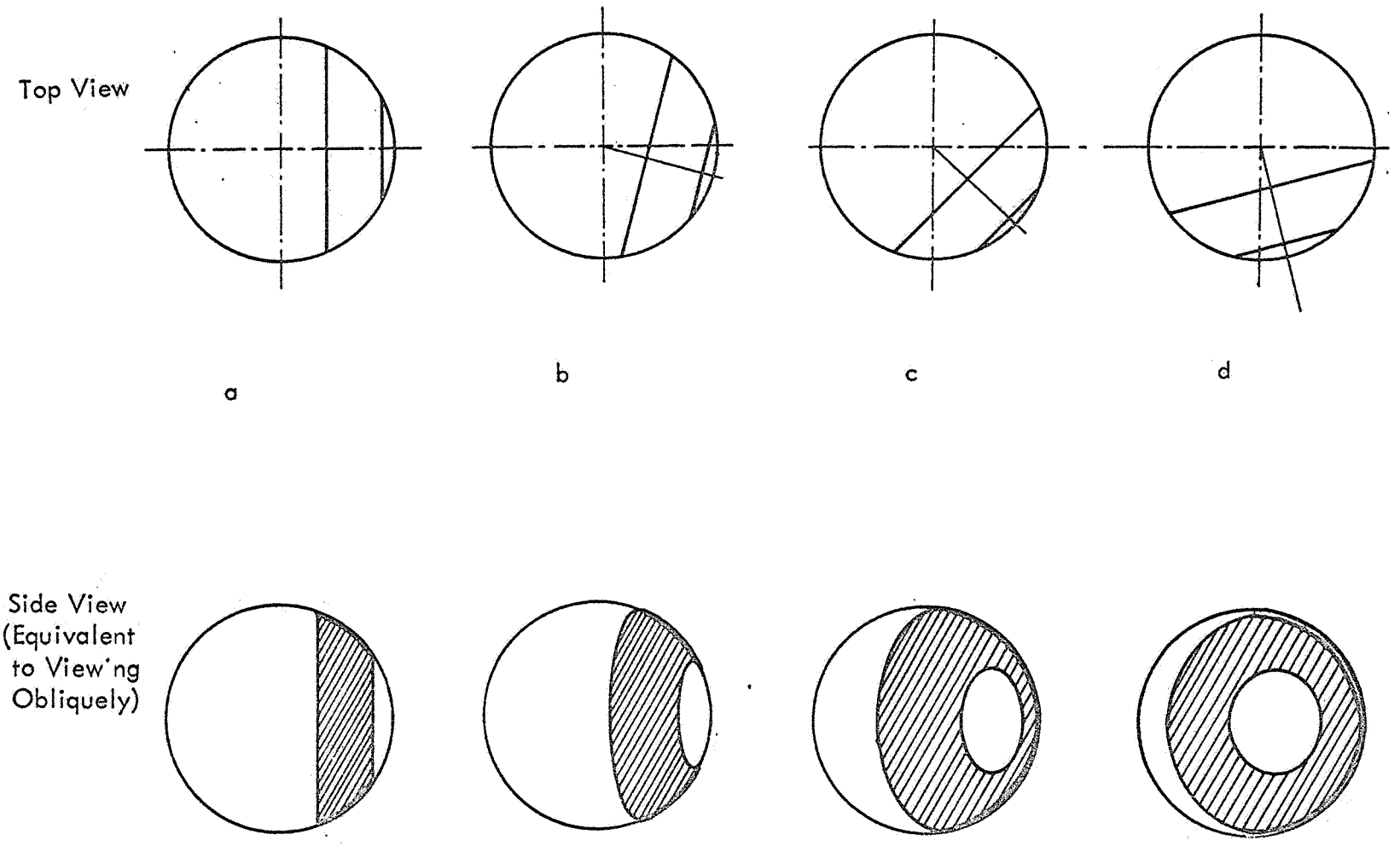

Figure 30. Diagram Showing Effect of Oblique Shadowgraphs

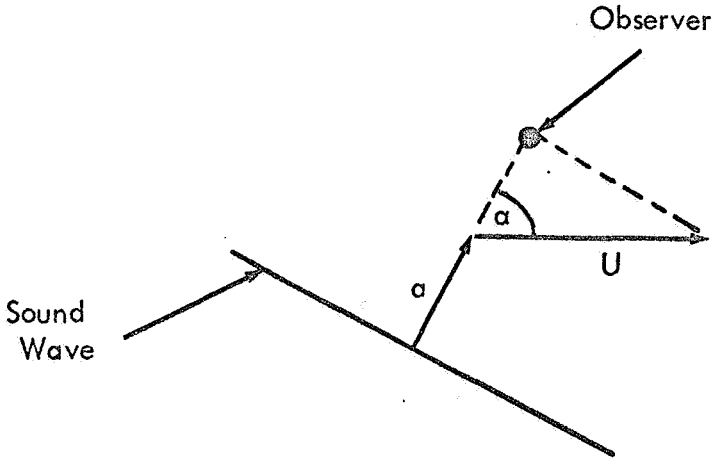

Figure 31. Velocity Diagram for Sound Waves

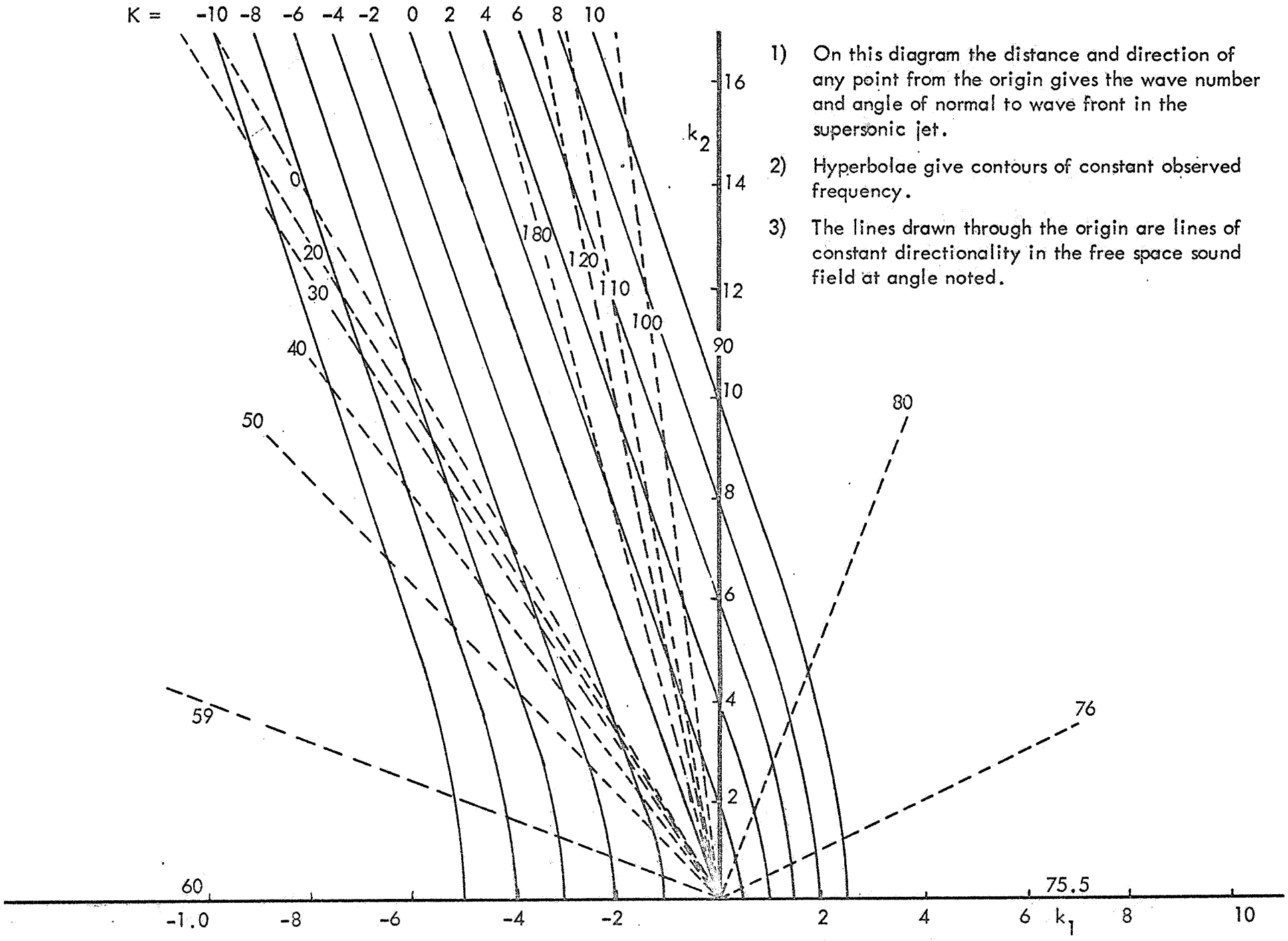

Figure 32. Frequency and Directionality Contours for Sound from a Supersonic Jet

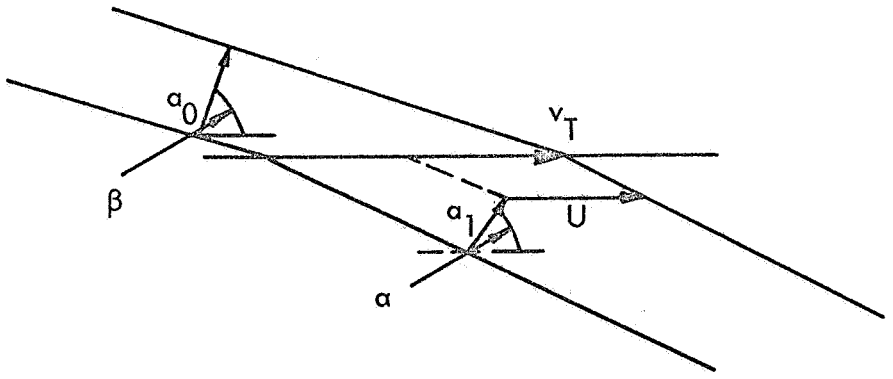

Figure 33. Refraction of Sound Waves at an Interface

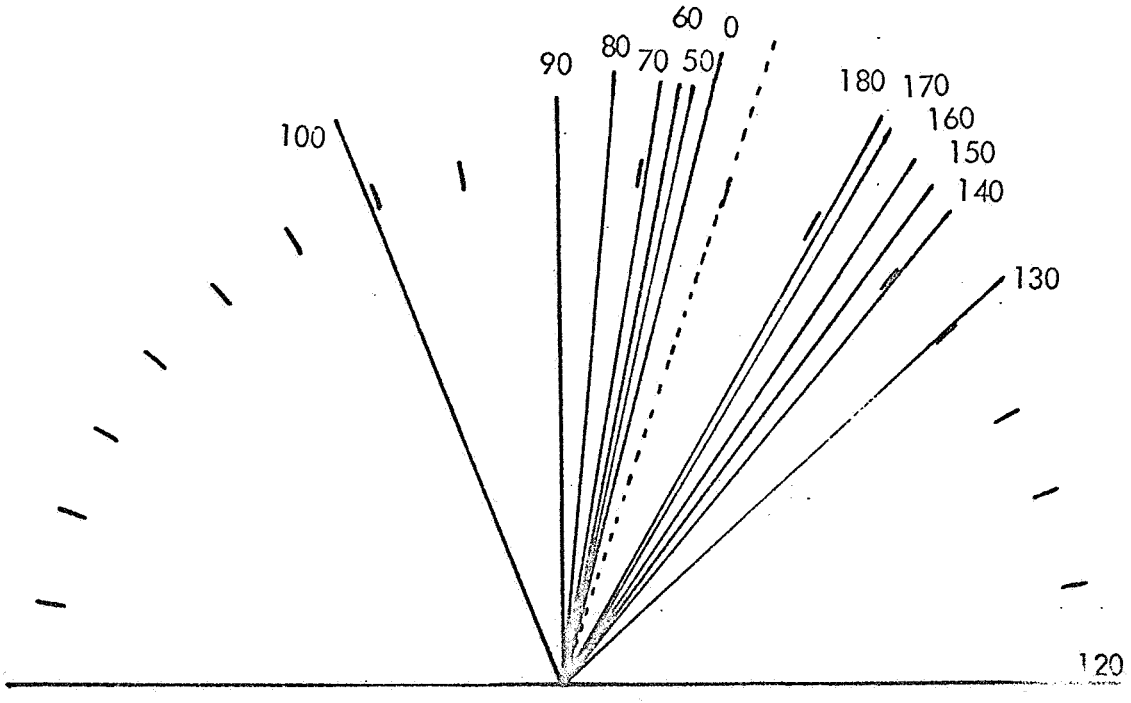

Figure 34. Alternative Diagram for Sound Radiation from Supersonic Jet

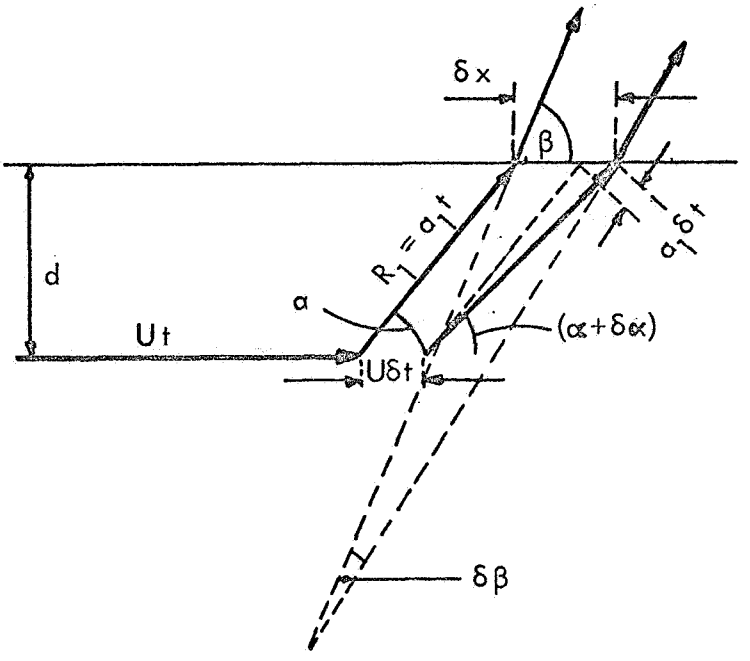

Figure 35. Refraction Diagram for Analysis of Curvature Effect